T-2328

PRESSURE BEHAVIOR OF HYDRAULICALLY FRACTURED OIL WELLS AT AND BELOW THE BUBBLE-POINT PRESSURE

by

John D. Wright

ProQuest LLC.
789 East Eisenhower Parkway
P.O. Box 1346
Ann Arbor, MI 48106 – 1346

T-2328

A Thesis submitted to the Faculty and Board of Trustees of the Colorado School of Mines in partial fulfillment of the requirements for the degree of Doctor of Philosophy, Petroleum Engineering.

Golden, Colorado
Date April 18, 1985

Signed: John D. Wright
John D. Wright

Approved: Daniel M. Bass
Dr. Daniel M. Bass
Thesis Advisor

Golden, Colorado
Date April 18, 1985

Craig W. Van Kirk
Dr. Craig W. Van Kirk
Head, Department of
Petroleum Engineering

ABSTRACT

Pressure transient analysis is widely used by the oil industry to determine in-situ rock properties, wellbore damage, and apparent fracture length in hydraulically fractured wells. These rock properties are used by engineers to analyze reservoir performance and to predict future production. The mathematical development of pressure transient analysis theory assumes single-phase, constant-compressibility fluids flowing in a radial system. Pressure transient tests of most oil wells do not meet these basic assumptions because the wells usually are hydraulically fractured, resulting in a non-radial flow system, and are in multiphase flow.

To investigate multiphase flow in hydraulically fractured wells, a two-phase, two-dimensional, finite-difference reservoir model was written to simulate an oil well. The well was produced below the bubble-point at a constant rate until pseudo-steady state flow conditions occurred in the reservoir. The well was then mathematically shut in and the well bore pressures were calculated during the buildup. These data were analyzed using the Horner method. The correct values for rock properties and fracture lengths can be calculated using the Horner method, provided a correction factor is applied as shown in this study.

TABLE OF CONTENTS

LIST OF FIGURES

LIST OF TABLES

This thesis is dedicated to my father,

John Samuel Wright

1898-1967

who wanted to attend the Colorado School of Mines but could never afford to, and who worked much of his life so that his son might have that opportunity.

ACKNOWLEDGMENTS

As with any enterprise which lasts well over a decade, there are numerous people and organizations who contributed to the author's (eventually) finishing this dissertation. I would like to acknowledge the help and support given to me by the following people: Professors Bill Astle, Don Dickinson, and Dr. Ramona Graves for serving on my committee; Sharon Dehmlow for her excellent job of typing; Dr. Dan Bass for originally suggesting the topic and acting as my advisor through the years; Dr. Craig W. Van Kirk, also a member of my committee, for his patience (even though he should have had less) and support, both financial and moral, and for believing that I would finish, even when I wasn't sure; Dr. Jim Crafton for taking the time to discuss technical matters and for caring enough to pump me up when I was down; Dr. Jack Krug for proofreading this report and for dragging me across the finish line; but mostly for being a friend, always ready to pour a scotch, light a cigar, and sponsor an attitude adjustment session.

A special thanks to my wife, Jane, whose unfailing optimism, cheerfulness, and giving nature saw me through the darkest days. We'll walk in the sunshine a bit more now.

∞

INTRODUCTION

Pressure transient analysis is widely used by the oil industry to determine in-situ rock properties, wellbore damage, and apparent fracture length in hydraulically fractured wells. These rock properties are used by engineers to analyze reservoir performance and to predict future production. The mathematical development of pressure transient analysis theory assumes single-phase, constant-compressibility fluids flowing in a radial system. Pressure transient tests of most oil wells do not meet these basic assumptions because the wells usually are hydraulically fractured, resulting in a non-radial flow system, and are in multiphase flow. The analysis techniques developed for single-phase radial systems must be modified if multiphase flow in fractured systems is to be correctly analyzed.

The pressure buildup test is the most widely used pressure transient test. To obtain meaningful data from a buildup test, the well must be produced at a known (and preferably constant) subsurface rate long enough to establish a stabilized pressure distribution. The well is then shut in and the bottom-hole pressure is recorded as a function of time. The data are then analyzed using the Horner method: the shut in pressures are plotted versus the

logarithm of flowing time plus shut in time divided by shut in time [$(t + \Delta t)/\Delta t$]. The slope of the straight-line portion of the data is proportional to the permeability of the formation. This method assumes single-phase, radial flow, and constant-compressibility fluid and rock.

Most of the literature on techniques for analyzing pressure transient tests of wells in multiphase flow has been for a radial geometry. Pressure transient tests of hydraulically fractured wells usually are discussed only for single-phase fluids. This study analyzes multiphase flow in hydraulically fractured wells using the Horner method. Furthermore, it demonstrates a method to determine the correct rock property values and the correct hydraulic fracture length.

To investigate multiphase flow in hydraulically fractured wells, a two-phase, two-dimensional, finite-difference reservoir model was written to simulate an oil well. The well was produced below the bubble point at a constant rate until pseudo-steady state flow conditions occurred in the reservoir. The well was then mathematically shut in, and the well bore pressures were calculated during the build-up. These data were analyzed using three currently available techniques: the log-pressure versus log-time type-curve-matching method, the pressure versus square-root-of-

time method, and the Horner method. The correct values for rock properties and fracture lengths can be calculated using the Horner method, provided a correction factor is applied as shown in this study.

LITERATURE SURVEY - Historical Development

One of the primary objectives of pressure transient analysis is to determine in-situ permeability, near wellbore damage, and average reservoir pressure. The history of pressure transient techniques for determining these properties is presented. In particular, this chapter traces the historical development of two branches of pressure transient analysis: 1) single-phase and multiphase flow and 2) artificially fractured wells.

Single-Phase and Multiphase Flow

The first published attempt to analyze pressure buildup curves was authored by Morris Muskat (1937). Based on his analysis of flow of an incompressible fluid, Muskat recommended plotting the logarithm of the external boundary pressure minus well flowing pressure ($P_e - P$) versus the shut in time (Δt). By varying the assumed value of P_e, the data can be made to plot as a straight line. The slope of the line is proportional to the permeability of the reservoir.

Evinger and Muskat (1942) discussed the calculation of a theoretical productivity index for the simultaneous flow of oil and gas. Together they developed the following equation defining steady-state flow in a reservoir.

$$q_o = \frac{2\pi\, k\, h}{\ln\left(\frac{r_e}{r_w}\right)} \int_{P_{wf}}^{P_e} \frac{k_{ro}}{\mu_o\, B_o}\, dP \qquad (1)$$

where

q_o = surface rate of oil production

k = permeability

h = height of producing formation

r_e = radius of external boundary

r_w = radius of wellbore

P_e = pressure at external boundary

P_{wf} = pressure at wellbore

k_{ro} = relative permeability to oil

μ_o = oil viscosity

B_o = oil formation-volume factor

Consistant units are used in the equation.

The Nomenclature section contains definitions of all the symbols used in the equations.

To analyze Equation 1, μ_o and B_o must be known functions of pressure. k_{ro} is related to pressure through the producing gas-oil ratio equation:

$$R = R_s + \frac{k_{rg}\, \mu_o\, B_o}{k_{ro}\, \mu_g\, B_g} \qquad (2)$$

where

R = producing gas-oil ratio

R_s = solution gas-oil ratio

k_{rg} = relative permeability to gas

μ_g = gas viscosity

B_g = gas formation volume factor.

By assuming a reservoir pressure and a gas-oil ratio, k_{rg}/k_{ro} is calculated. Because k_{rg}/k_{ro} is a function of S_o, a value of S_o is thereby determined. kro is then determined from the relative permeability curves. All the variables in the integral are now known functions of pressure and the integral is evaluated numerically. Evinger and Muskat followed this procedure and calculated various cases with differing pressures and gas-oil ratios. They showed the productivity index (PI, BOPD/psi) for their two-phase systems varied with pressure drawdown. This change in PI with drawdown is in contrast to single-phase theory where PI is constant. Although Evinger and Muskat's work assumed steady-state conditions, its applicability to transient flow will be discussed later.

The results of Evinger and Muskat's work were not applied by the petroleum industry for 30 years. In the

meantime, the development of pressure transient analysis followed other paths.

Miller, Dyes, and Hutchinson (1950) derived a method of analyzing pressure transient tests which included the effects of compressibility. They concluded that a plot of shut in pressure versus the logarithm of shut in time would form a straight line during much of the shut in time, and furthermore, that the reservoir permeability is proportional to the slope of the line. Permeability can be calculated from Equation 3.

$$k = \frac{162.5\ q\mu B}{mh} \qquad (3)$$

where

m = slope of straight line portion of semi-log plot, psi/cycle.

This equation, with the constant changed to 162.6, is one of today's fundamental pressure transient analysis equations.

Miller, Dyes, and Hutchinson (MDH) also investigated the effects of wellbore storage, skin damage, and multiphase flow using an electric analyzer. In addition, they presented a method to calculate the average reservoir pressure

measurements. They were also the first investigators to define the dimensionless pressure and dimensionless time functions. These dimensionless variables form the foundation of much of the modern methodology of pressure transient analysis. Dimensionless pressure is defined by Equation 4.

$$P_D = \frac{kh\ (P_i - P_{wf})}{141.2\ q\mu B} \tag{4}$$

where

P_i = initial pressure

And dimensionless time is defined by Equation 5.

$$t_D = \frac{.0002637\ kt}{\phi\ \mu\ c\ r_e^2} \tag{5}$$

where

c = compressibility, psi^{-1}

ϕ = porosity, decimal

t = time, hours.

Multiphase flow requires modifying Equations 4 and 5. The $q\mu B$ term in Equation 4 becomes $q_L\mu_L B_L$ and Equation 5 becomes

$$t_D = \frac{0.0002637\ k}{\phi\ \mu_L\ c_t\ r_e^2} \left(\frac{\gamma_L + \gamma_g\ R/5.615}{B_o\ \gamma_t}\right) t \qquad (6)$$

where

γ_L = specific weight of liquid

γ_g = specific weight of gas

γ_t = specific weight of mixture.

R = "gas-oil ratio"

MDH provided a simple method of calculating permeability from a pressure buildup test. However, the MDH method is valid only if the well has produced for a long time compared to the shut in time ($t >> \Delta t$).

Horner (1951) removed this restriction and showed the shut in pressure versus the log $[(t + \Delta t)/\Delta t]$ plots as a straight line which can be analyzed using Equation 3, even if the shut in time is nearly the same as the producing time. Horner investigated pressure buildup tests of a single well in an infinite reservoir. He also investigated the effect of a linear barrier in an otherwise infinite reservoir. He showed that the straight line portion of the curve can be extrapolated to infinite shut in time. In an infinite reservoir the pressure at infinite shut in time (P*) represents the initial reservoir pressure. In a finite reservoir, P* is a "false" pressure and must be corrected to

obtain the static pressure ($\bar{P}$).

Horner derived the following equation to obtain the correct static pressure.

$$\bar{P} = P_i - \frac{q\,\mu}{4\pi\,kh}\left\{\ln\left(\frac{t+\Delta t}{\Delta t}\right) - Y(t+\Delta t) + Y(\Delta t)\right\} \qquad (7)$$

where

Δt = shut in time

and

Y is a complex function of r_w/r_e and

$\frac{\phi\mu c r_e^2}{kt}$ involving a summation of Bessel functions and other terms.

He simplified this equation and demonstrated a method of calculating $\bar{P}$. The Horner plot is today's "conventional" means of analyzing pressure buildup tests.

Matthews, Brons, and Hazebroek (1954) extended Horner's method for calculating the average reservoir pressure in an infinite reservoir to a finite reservoir with various drainage shapes and well locations. They derived an analytical expression for $(P^* - \bar{P})/(q\mu/4\pi kh)$ assuming $r_w^2/r_e^2 \cong 0$ (i.e. $r_e >> r_w$). Values of the function were calculated for a range of $\frac{kt}{\phi\mu cA}$ and different drainage shapes.

Although Miller, Dyes, and Hutchinson attempted to consider zones of increased or decreased permeability near the wellbore, it is van Everdingen (1953) who is credited with the term "skin effect" for a zone of reduced (or increased) permeability of infinitesimal radius surrounding the wellbore. A positive skin indicates a lower permeability zone (or damage) surrounding the wellbore, while a negative skin indicates a higher (or enhanced) permeability zone near the well. In 1953, hydraulic fracturing was in its infancy and van Everdingen's main concern was analyzing acid stimulation treatments. Today, the skin factor concept is used in analyzing pressure buildup tests in hydraulically fractured wells even though the induced hydraulic fracture is obviously not a "skin" phenomenon.

Perrine (1956) once again addressed the question of multiphase flow. He suggested that total mobility (k_t/μ_t), compressibility (c_t), and production rate (q_t) be substituted for their single-phase counterparts and that a standard Horner, van Everdingen, or Matthews, Brons, and Hazebroek analysis be performed. The oil, gas, and water effective permeabilies are obtained by solving Equation 3 for each phase. Perrine justified this methodology based upon a digital computer study. His published results indicate that an unfractured well can be analyzed using this

technique. Martin (1959) provided a theoretical basis for the equations presented by Perrine. Weller (1965) confirmed that Perrine's method is applicable in unfractured reservoirs. Earlougher, et al., (1967) confirmed Perrine's method is applicable in unfractured reservoirs containing two wells.

Fetkovich (1973) suggested isochronal tests be run on oil wells as well as gas wells. He resurrected the 1942 Evinger and Muskat multiphase flow theory and, for steady-state flow, calculated the oil rate from:

$$q_o = \frac{.00708\ kh}{\ln(\frac{r_e}{r_w})} \int_{P_{wf}}^{P_e} \frac{k_{ro}}{\mu_o B_o} dP \quad . \tag{8}$$

Fetkovich extended this same concept to transient flow. Oil rate as a function of time for transient flow is calculated from Equation 9.

$$q_o = \frac{kh}{141.2\ (.5\ \ln t_D + .404 + s')} \{m(P_i) - m(P_{wf})\} \tag{9}$$

where

s' = total skin factor

and

m(P) is the oil pseudo-pressure defined by Equation 10.

$$m(P) = \int_{P_b}^{P} \frac{k_{ro}(S_o)}{\mu_o B_o} dP \qquad (10)$$

The dimensionless time is defined by Equation 11.

$$t_D = \frac{0.0002637\ kt}{\phi\ \mu_{oi}\ c_{ti}\ r_w^2} \quad . \qquad (11)$$

In Equation 9, s' is a skin effect which includes wellbore damage and the increased resistance to oil flow caused by the development of a gas saturation around the wellbore.

It remained for Raghavan (1976) to present these equations in an understandable and useable form. Raghavan noted that even though k_{ro} is really a function of saturation, not pressure, the integral defining m(P) could be evaluated by using producing GOR to relate the pressure and saturation terms. He provided a step-by-step procedure to calculate m(P) for an oil well, which is reproduced below.

1. Tabulate t, P, and R in appropriate units.
2. Using tabulated values of P and R, calculate k_g/k_o using the following equation.

$$R = R_s + \frac{k_g\ \mu_o\ B_o}{k_o\ \mu_g\ B_g} , \qquad (12)$$

3. From relative-permeability curves calculate k_g/k_o as a function of S_o.
4. From Steps 2 and 3 determine P versus S_o.
5. From knowledge of P versus S_o obtain k_{ro} versus P using relative permeability data.
6. Calculate m(P) by numerical integration using the relation obtained in Step 5 and PVT data.

Using a reservoir simulator, Raghavan modeled a radial flow system during drawdown and buildup. In the case he studied, the dimensionless pressure versus dimensionless time data followed the theoretical solution for a slightly compressible fluid for most of the drawdown. He noted that the results were sensitive to flow rate. When m(P) is plotted against dimensionless time, the difference between the two solutions is negligible during the early transient period. During the pseudo-steady state period, there is a large difference between the two solutions. From the figures in his paper, it appears that the dimensionless pressure solution is much closer to the theoretical solution, at least for the data he used. He also investigated using m(P) during the buildup. He found that m(P) must be constructed using the producing GOR at the instant the well is shut in. The value of absolute permeability calculated from the buildup was

within 7 percent of the known value. Raghavan also found using m(P) during drawdown resulted in determining the proper magnitude of skin damage. If pressure is used instead of m(P), the calculated skin appears to be much greater than the real skin because of the increased gas saturation around the wellbore.

Fetkovich's and Raghavan's work represent the latest concepts in multiphase pressure transient analysis.

Hydraulically Fractured Wells

Prats (1960) was the first investigator to study pressure transient behavior in vertically fractured wells. He used conformal mapping techniques to transform an elliptical system into a linear system. He then solved Laplace's equation using a Fourier series technique. Because of the use of Laplace's equation, his results assume steady-state conditions. He concluded that a large capacity vertical fracture can be simulated as a radial flow system with a wellbore radius equal to one-half of the fracture half-length provided the relative fracture capacity "a" is less than 0.1 where "a" is defined by:

$$a = \frac{\pi}{2} \frac{k}{k_f} \frac{x_f}{w_f} \quad . \tag{13}$$

and k_f = permeability of fracture

W_f = width of fracture

For values of "a" greater than 0.1, the equivalent wellbore radius decreases rapidly. Thus, an infinite or almost infinite conductivity fracture behaves in steady-state flow as a radial system with $r_w = 0.5\ x_f$.

A year later (1961), Prats, in conjunction with Hazebroek and Strickler, published the results of a study of compressible fluid flow into vertically fractured wells. Once again they transformed an elliptical system into a linear system, and solved the equations with the use of Laplace's transforms. The resulting series of equations are not useful for early production history, and the results are only applicable to semi-steady state conditions. Prats again concluded that a fractured system can be reasonably represented by a radial system with a wellbore radius of 1/2 the fracture half-length, provided a small error is acceptable. In the case of compressible flow, there is up to a seven percent error. In the incompressible case, the equivalence is exact. These results are valid only for fracture half lengths less than 1/2 the radius of drainage. For fracture half-lengths greater than this value, the errors become quite large for compressible and incompressible fluids.

Prats and Levine (1963) applied this theory to multiphase flow. Again, the fractured well was shown to be essentially equivalent to a circular reservoir with the wellbore radius equal to 1/2 the fracture half-length during semi-steady state flow.

Scott (1963) was the first to study transient flow in vertical fractures. He used a physical heat-flow model to simulate a reservoir with a fracture half-length equal to 0.182 r_e. For a high capacity fracture, he found that transient flow in a vertically fractured well can be modeled as proposed by Prats.

The following year, Russell and Truitt (1964) used a mathematical computer model to simulate a fractured well. They found the permeabilities calculated using the Horner method were much too high. The amount of error was correlated with the fracture penetration. (See Figure 1 for their results.) Russell and Truitt also showed there was no "truly" linear section on the buildup curves. The smaller the fracture, the closer the pressure transients approach radial flow theory. They also found the calculated fracture penetration to be too small. The ratio of calculated- to actual-fracture penetration was also correlated with actual fracture penetration, as shown in Figure 2. Use of Figure 2 requires a trial and error solution for fracture penetration.

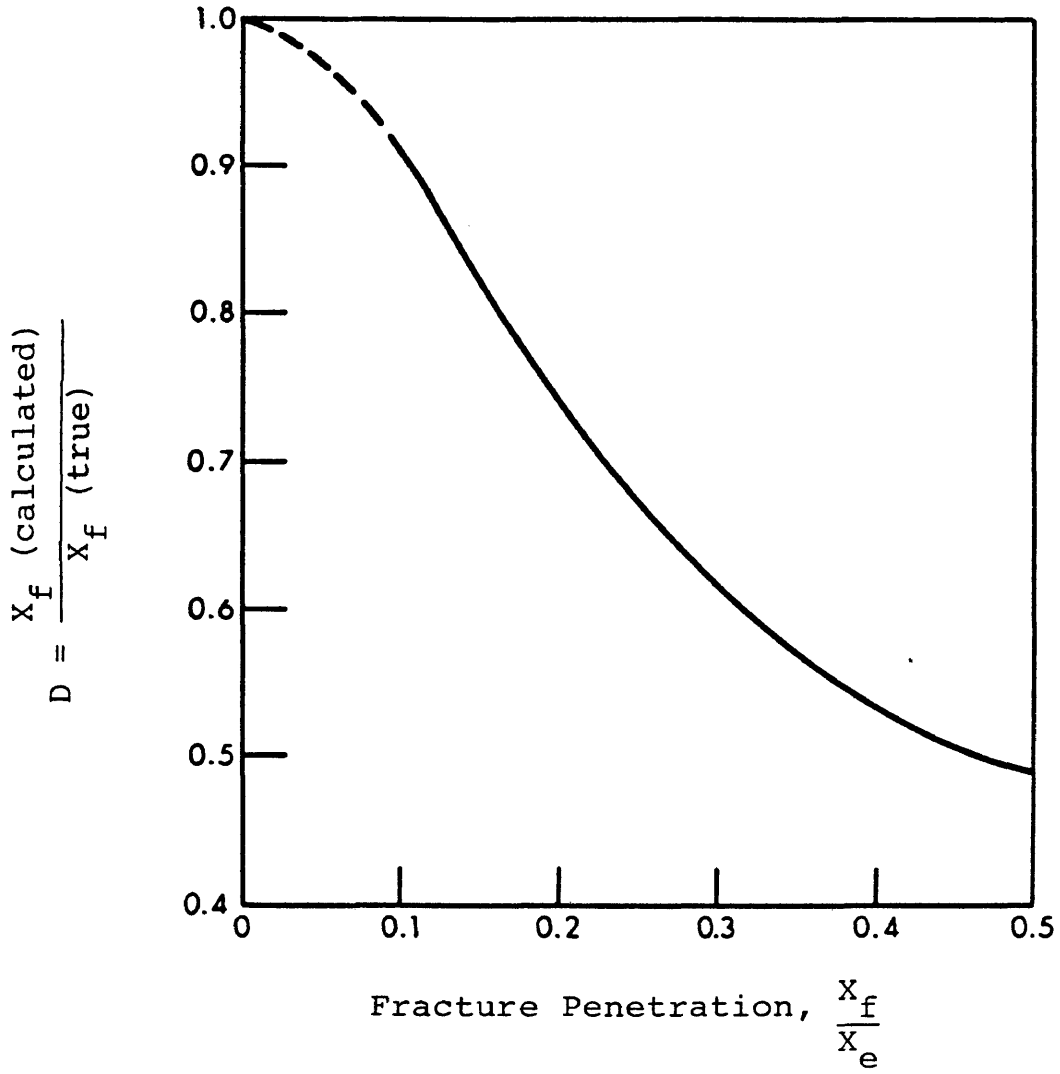

Figure 1. Effect of Fracture Penetration on Fracture Length as Derived from Skin Factor Formula (Pressure Build-Up) (from Russell and Truitt, 1964).

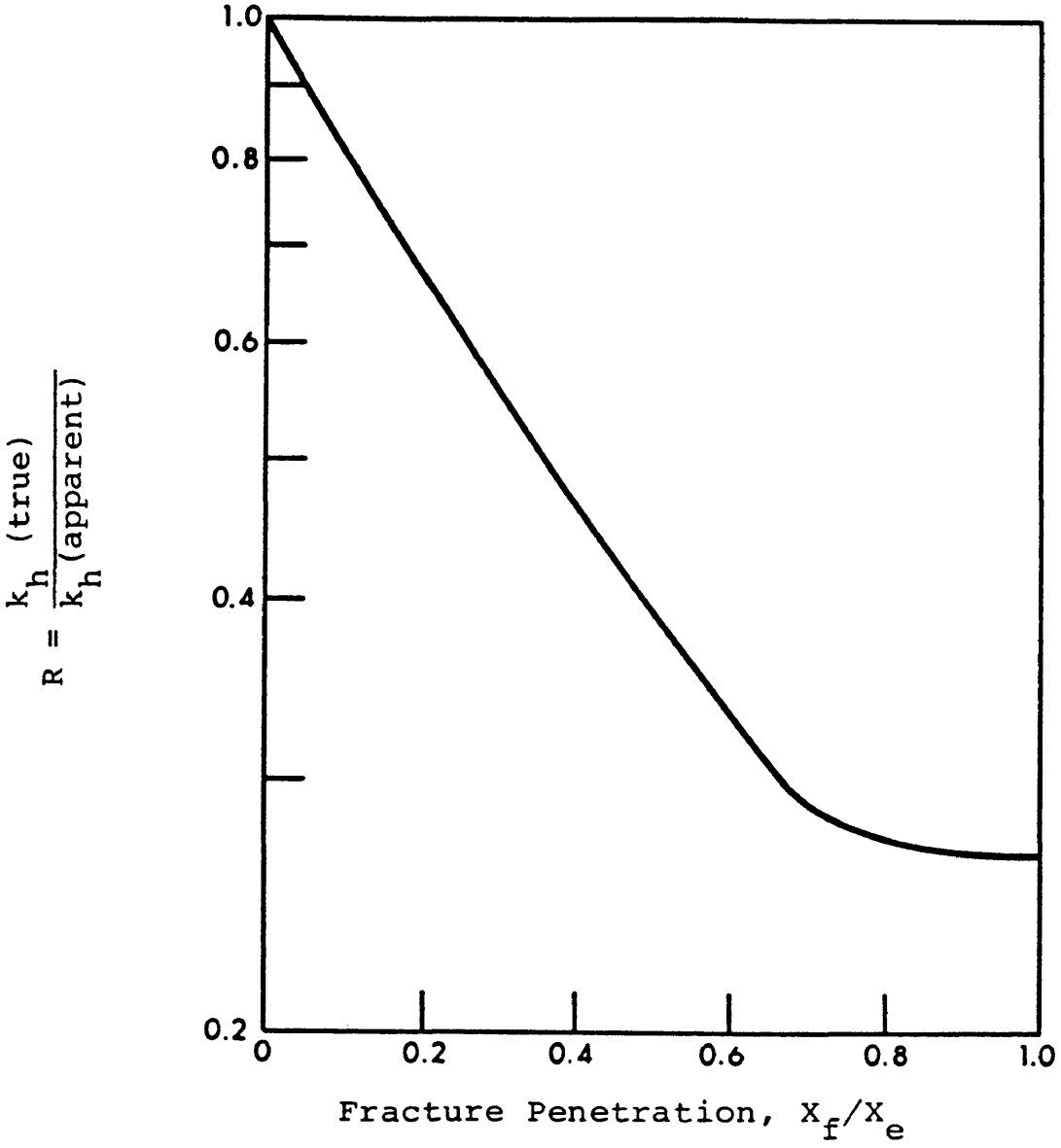

Figure 2. Vertically Fractured Reservoir, Pressure Build-Up Interpretation, kh Magnification Factor vs. Fracture Penetration (from Russell and Truitt, 1964).

Ramey and Cobb (1971) presented a discussion of general buildup theory for wells in a closed drainage area. They observed that the Muskat technique is applicable only during late times. They recommended Horner's method for determining permeability and skin effect.

Raghavan, Cady, and Ramey (1972) confirmed and extended Russell and Truitt's findings. They showed that Horner plots are best for determining permeability and, when properly used, Muskat plots are useful for determining the static reservoir pressure. Raghavan, et al., found the calculated permeability had to be corrected similarly to the procedure proposed by Russell and Truitt. Figure 3 extends the results of Russell and Truitt to Miller, Dyes, and Hutchinson plots.

Gringarten, Ramey, and Raghavan (1972) developed analytical expressions for vertically and horizontally fractured wells. They published dimensionless curves for both uniform flux and infinite conductivity fractures, which are shown in Figures 4 through 6. The infinite conductivity solution assumes the pressure in the fracture is everywhere the same. Since the pressure in the reservoir is higher near the end of the fracture, it follows that more fluid per unit length enters the fracture near the tip than enters near the wellbore. The constant flux solution assumes that

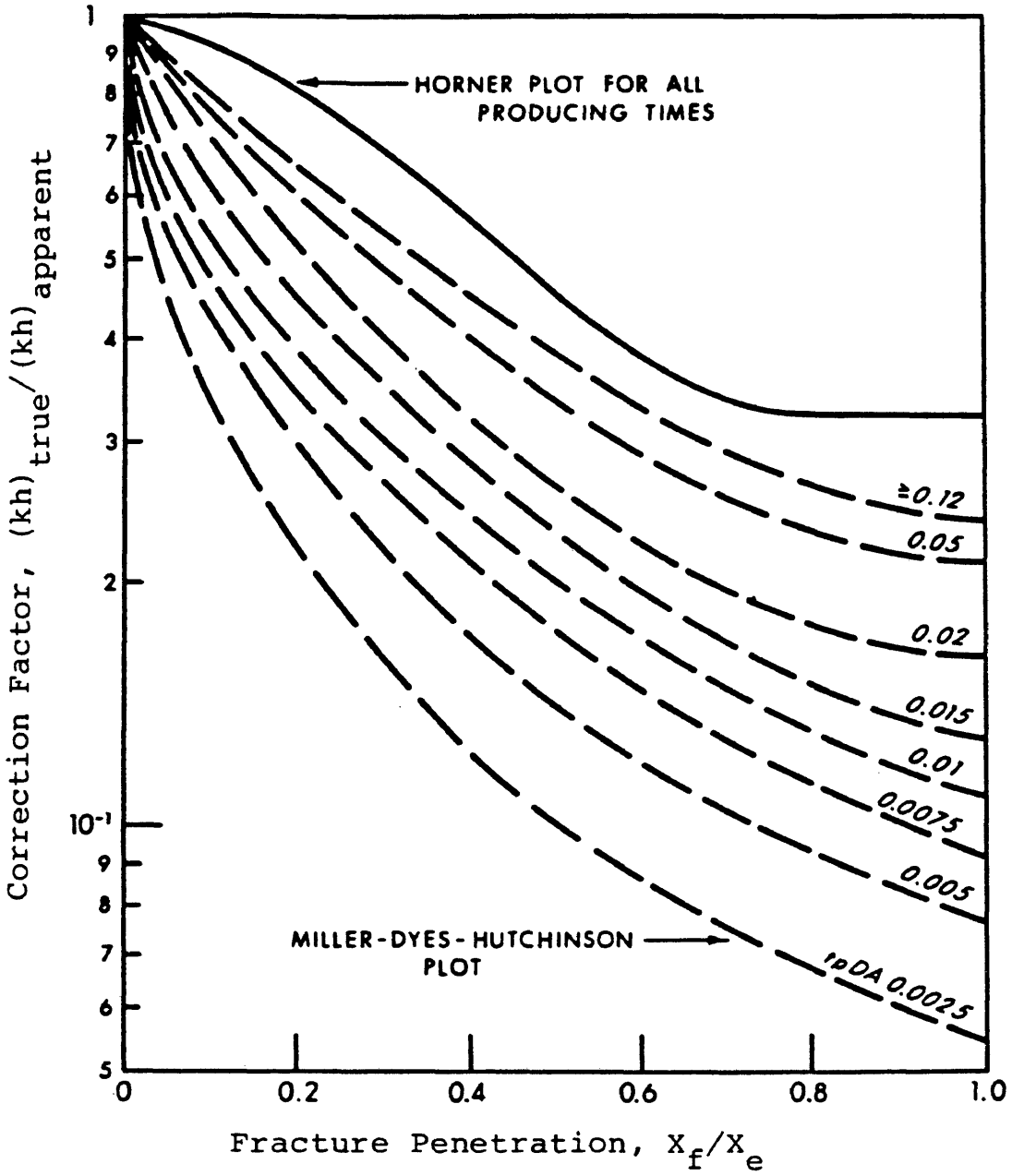

Figure 3. Correction Factor for kh estimated from pressure build-up tests in vertically fractured wells, assuming sufficient shut-in time to reach maximum slope (from Raghavan, Cady, and Ramey, 1972).

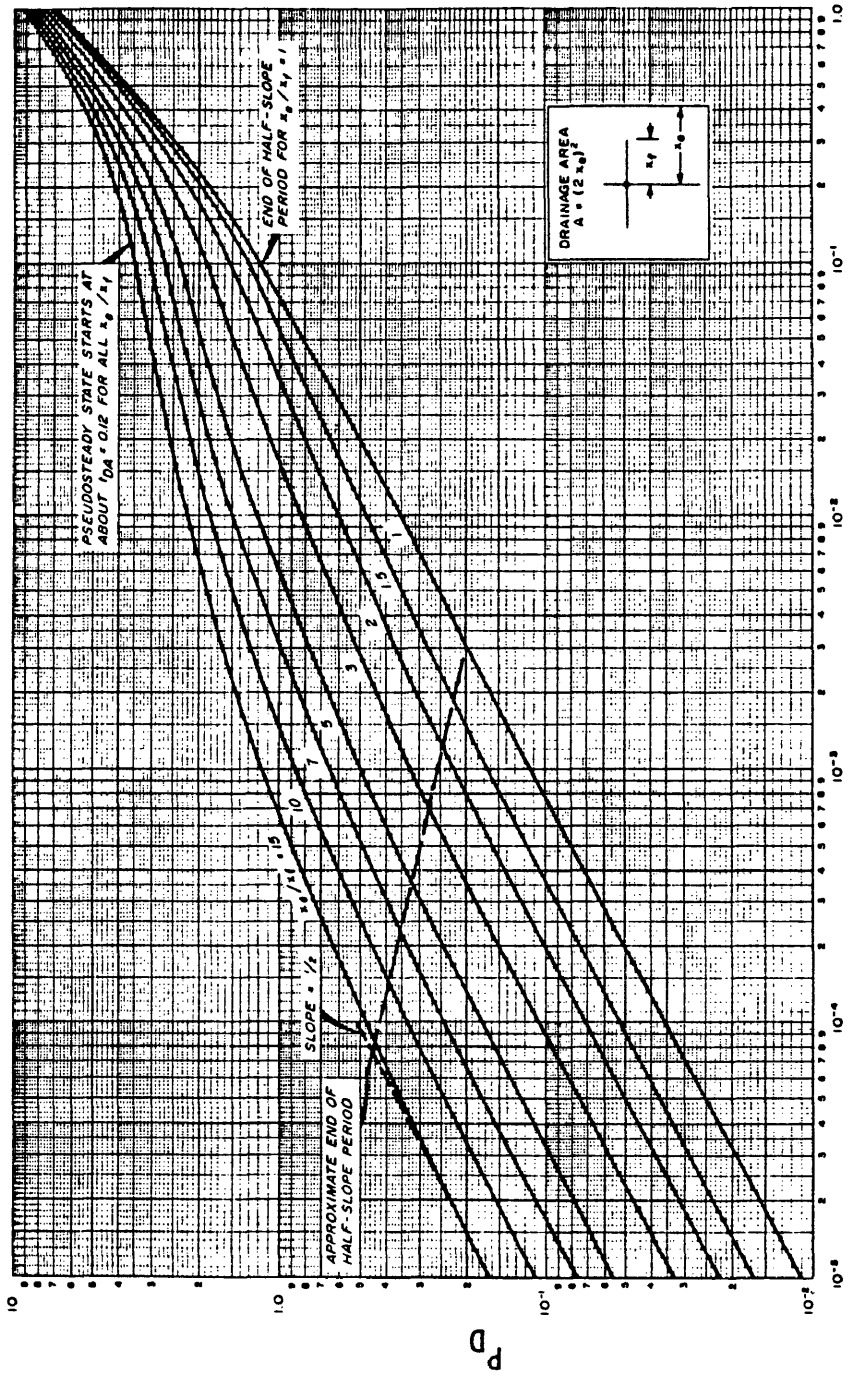

Figure 4 - Dimensionless pressure for vertically fractured well in the center of a closed square, no wellbore storage, infinite-conductivity fracture. (from Earlougher, 1977, p 216)

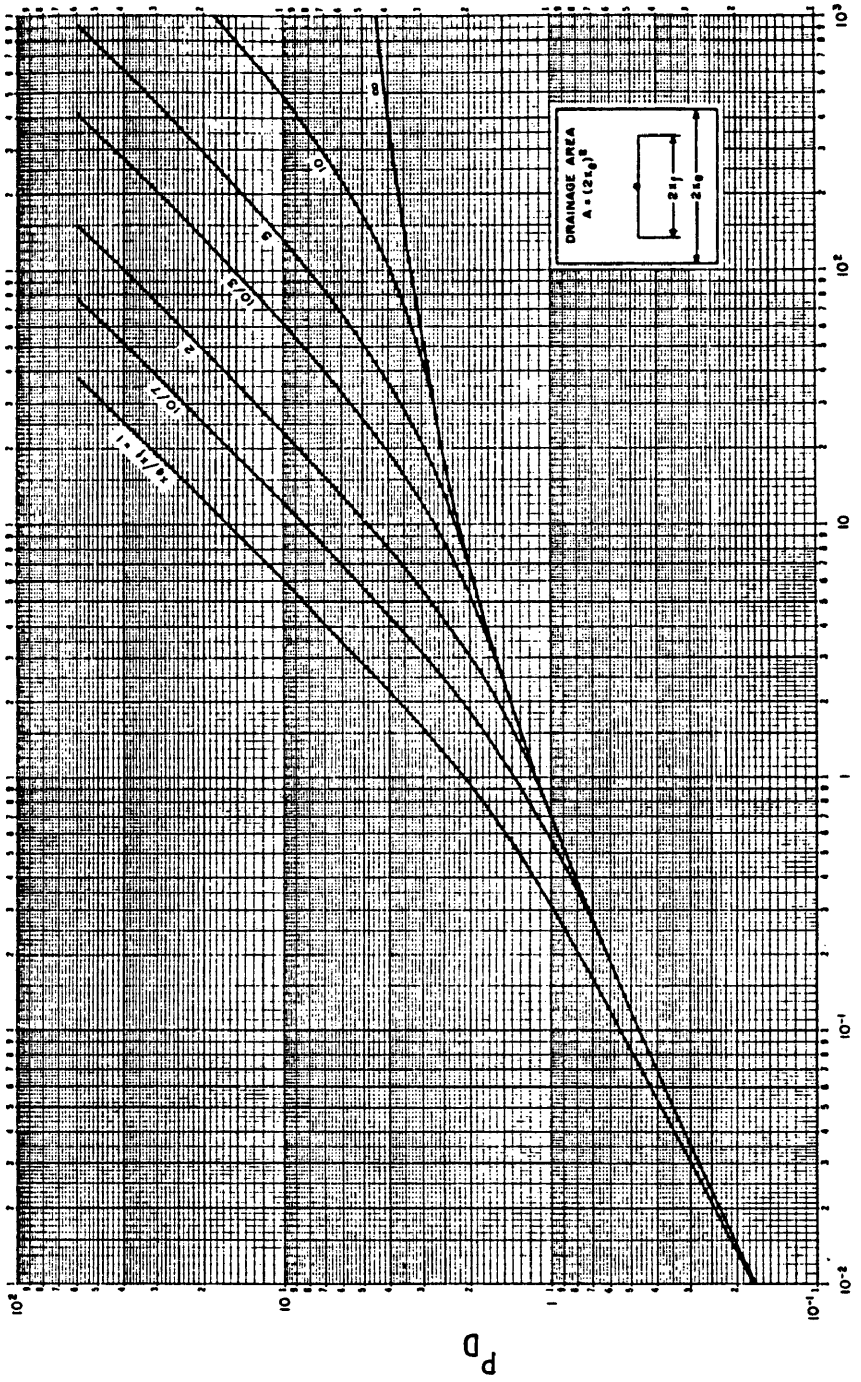

Figure 5 - Dimensionless pressure for vertically fractured well in the center of a closed square, no wellbore storage, infinite-conductivity fracture. (from Earlougher, 1977, p 217)

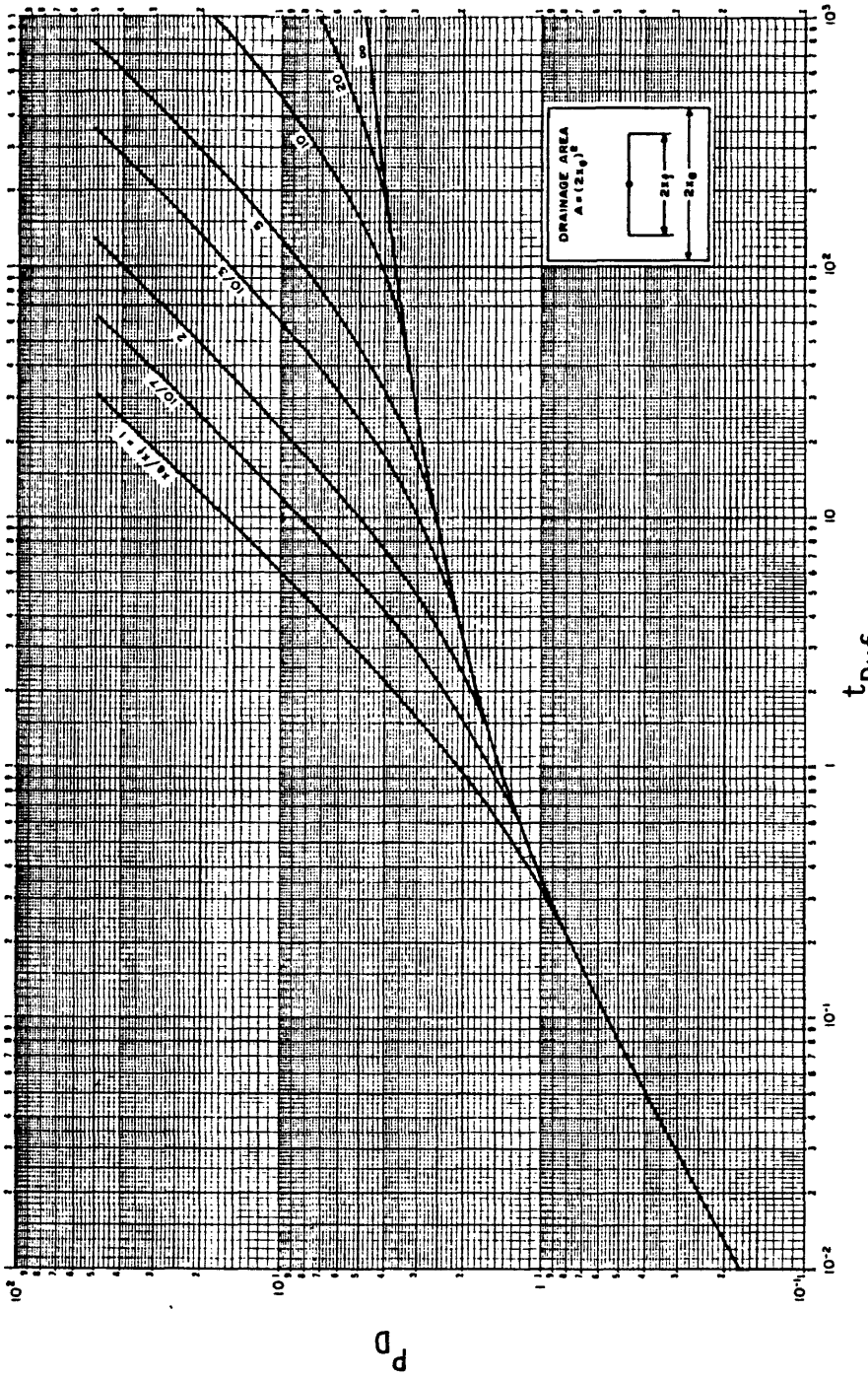

Figure 6 - Dimensionless pressure for vertically fractured well in the center of a closed square, no wellbore storage, uniform-flux fracture. (from Earlougher, 1977, p218)

the same amount of fluid per unit length enters the fracture at all points. In order for this to occur, the difference in pressure between the reservoir and the fracture must be constant at all points in the fracture. Since the pressure in the reservoir is higher near the end of the fracture, this implies that there is a pressure drop in the fracture. Figure 7, from Gringarten, et al., illustrates the difference in flux for an infinite conductivity and constant flux fracture. Gringarten, et al., also recommended using type curve matching to calculate permeability and fracture half-length.

Gringarten, Ramey and Raghavan (1975) presented an application of their method. They stated that the infinite conductivity fracture assumption appears to match field tests for artificially fractured wells, while the constant flux solution appears to match naturally fractured systems.

Raghavan and Hadinoto (1976) investigated a fractured well with a constant-pressure outer boundary. They presented an equation relating the effective wellbore radius to the fracture penetration.

Raghavan (1977) was the first to investigate multiphase transient flow in artifically fractured reservoirs. His study was an extension of the simulation of a radial system discussed earlier. Using a reservoir simulator, he

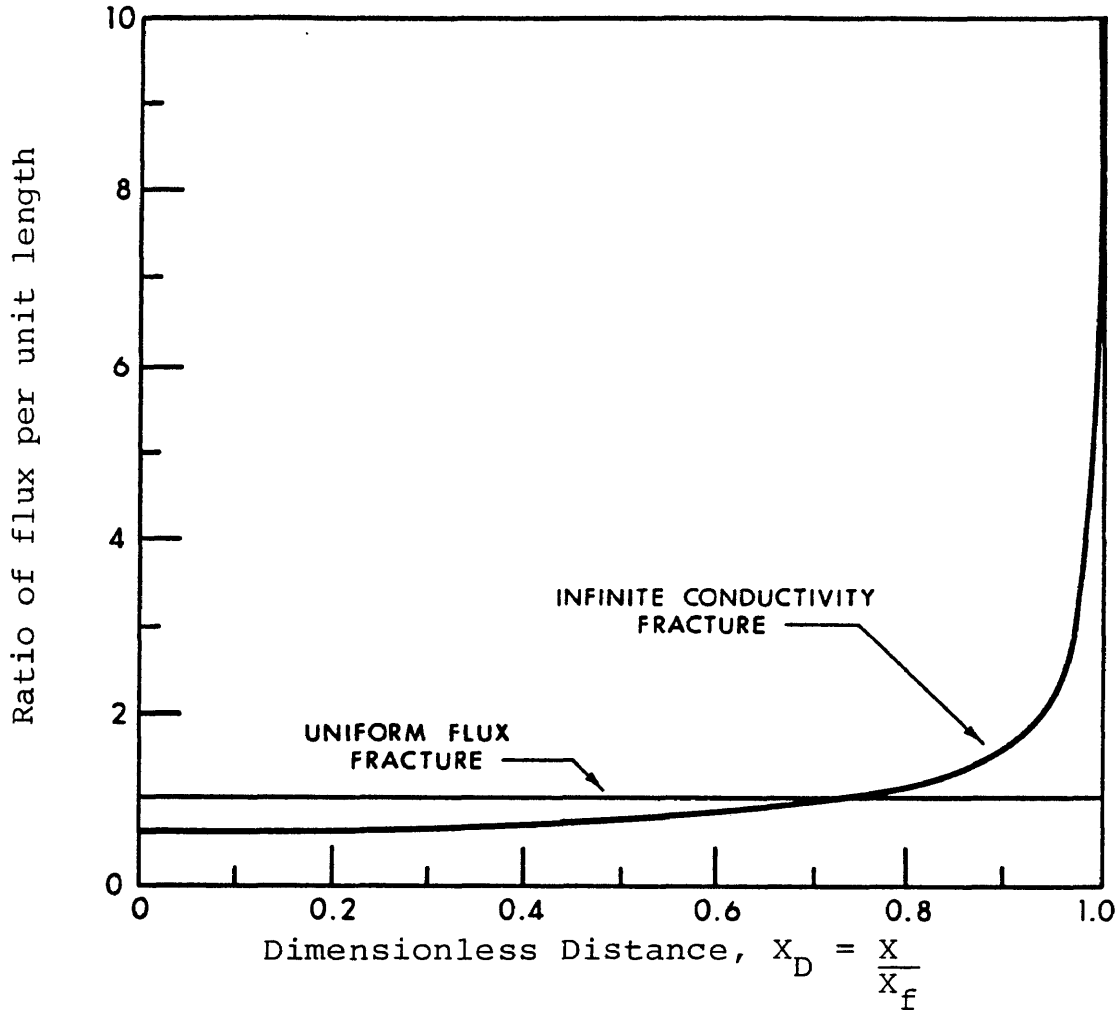

Figure 7. Production flux along vertical fracture (from Gringarten, Ramey, and Raghavan, 1972).

investigated the drawdown behavior of a well, assuming three different fracture penetration ratios (X_f/X_e of 0.2, 0.5, 1.0). He also investigated pressure buildup for the system at an X_f/X_e ratio of 0.2 and three different gas saturations (0.75 percent, 9.3 percent, and 15 percent). He used the relative permeability data, PVT data, and much of the rest of the reservoir data from his earlier study. During drawdown, he found that the log m(P) versus log t curve followed the constant compressibility solutions until pseudo-steady state flow occurred. Beyond this time, the match was not good. During pressure buildup, he found that the standard Horner plot of pressure versus Horner time resulted in reasonable values for oil permeability, but calculated fracture lengths were considerably too small when the gas saturation in the reservoir was large. He recommended using m(P) to evaluate the pressure buildup and found, as he had in radial flow, that the GOR at the time of shut in must be used to calculate m(P). When this is done, he stated that the type curve matching method results in acceptable values of both absolute permeability and fracture length.

COMPUTER MODEL

A generalized two-dimensional, two-phase reservoir simulator with rectangular coordinates was written and used in this study. Details of the simulator's mathematical formulation are contained in Appendix A. The simulator is similar to the one described by Breitenbach, Thurnau, and vanPoollen (1969a,b,c,d). It is an IMPES simulator which means the pressures at the new time level are determined implicitly and then the saturations are updated explicitly. This solution technique is not an elegant method of solving single-well problems; however, it is relatively easy to program, stable, and when correctly applied, yields excellent answers. The main drawback to the IMPES formulation is the explicit solution for saturations. This solution technique requires very small timesteps (less than 0.1 days) when the gas phase becomes mobile. Methods exist which reputedly solve for saturations in a semi-implicit manner (MacDonald and Coats, 1970; Letkeman and Ridings, 1970) or fully-implicit manner (Aziz and Settari, 1979, p. 164). These methods are inherently more stable than IMPES, and thereby should allow larger timesteps and ultimately less computing time. The IMPES, simi-implicit, and fully-implicit methods were programmed and simulation runs

were made using all three solution techniques. Although identical answers were obtained for all three methods, it was not possible to increase the timestep size and retain stability for the semi-implicit or the fully-implicit solution methods. It is not known whether this lack of stability is because of the unusual geometry of the problem or faulty programming. The development and verification of a fully-implicit simulator is suggested for future studies of single-well problems.

Method Of Pressure Solution.

The two-dimensional, implicit pressure formulation results in a pentadiagonal matrix: See Figure 8. A number of methods exists to solve this matrix, i.e. Gausian elimination, ADIP, LSOR, SIP, etc. Most of these methods are iterative techniques. Two methods, line successive over-relaxation (LSOR), and Gausian elimination, were programmed. The BANDSOLVE algorithm presented by Thurnau (1963) was used to perform the Gausian elimination. This algorithm is considerably faster than LSOR (Breitenbach, Thurnau, vanPoollen, 1969c) for the size of problem (less than 17 by 18 cells) and tolerances desired (less than 0.001 psi). BANDSOLVE has two major advantages: the code is published and readily available, and the results are

Row	Column 01	02	03	04	05	06	07	08	09	10	11	12	13	14	15	16	17	18	19	20	21	22	23	24	25	26	27	28
01	X	X	.	.	X	.	.	.	.	.	.	.	.	.	.	.	.	.	.	.	.	.	.	.	.	.	.	.
02	X	X	X	.	.	X	.	.	.	.	.	.	.	.	.	.	.	.	.	.	.	.	.	.	.	.	.	.
03	.	X	X	X	.	.	X	.	.	.	.	.	.	.	.	.	.	.	.	.	.	.	.	.	.	.	.	.
04	.	.	X	X	.	.	.	X	.	.	.	.	.	.	.	.	.	.	.	.	.	.	.	.	.	.	.	.
05	X	.	.	.	X	X	.	.	X	.	.	.	.	.	.	.	.	.	.	.	.	.	.	.	.	.	.	.
06	.	X	.	.	X	X	X	.	.	X	.	.	.	.	.	.	.	.	.	.	.	.	.	.	.	.	.	.
07	.	.	X	.	.	X	X	X	.	.	X	.	.	.	.	.	.	.	.	.	.	.	.	.	.	.	.	.
08	.	.	.	X	.	.	X	X	.	.	.	X	.	.	.	.	.	.	.	.	.	.	.	.	.	.	.	.
09	.	.	.	.	X	.	.	X	X	.	.	.	X	.	.	.	.	.	.	.	.	.	.	.	.	.	.	.
10	.	.	.	.	.	X	.	.	.	X	X	.	.	X	.	.	.	.	.	.	.	.	.	.	.	.	.	.
11	.	.	.	.	.	.	X	.	.	X	X	X	.	.	X	.	.	.	.	.	.	.	.	.	.	.	.	.
12	.	.	.	.	.	.	.	X	.	.	X	X	X	.	.	X	.	.	.	.	.	.	.	.	.	.	.	.
13	.	.	.	.	.	.	.	.	X	.	.	X	X	.	.	.	X	.	.	.	.	.	.	.	.	.	.	.
14	.	.	.	.	.	.	.	.	.	X	.	.	.	X	X	.	.	X	.	.	.	.	.	.	.	.	.	.
15	.	.	.	.	.	.	.	.	.	.	X	.	.	X	X	X	.	.	X	.	.	.	.	.	.	.	.	.
16	.	.	.	.	.	.	.	.	.	.	.	X	.	.	X	X	X	.	.	X	.	.	.	.	.	.	.	.
17	.	.	.	.	.	.	.	.	.	.	.	.	X	.	.	X	X	.	.	.	X	.	.	.	.	.	.	.
18	.	.	.	.	.	.	.	.	.	.	.	.	.	X	.	.	.	X	X	.	.	X	.	.	.	.	.	.
19	.	.	.	.	.	.	.	.	.	.	.	.	.	.	X	.	.	X	X	X	.	.	X	.	.	.	.	.
20	.	.	.	.	.	.	.	.	.	.	.	.	.	.	.	X	.	.	X	X	X	.	.	X	.	.	.	.
21	.	.	.	.	.	.	.	.	.	.	.	.	.	.	.	.	X	.	.	X	X	.	.	.	X	.	.	.
22	.	.	.	.	.	.	.	.	.	.	.	.	.	.	.	.	.	X	.	.	.	X	X	.	.	X	.	.
23	.	.	.	.	.	.	.	.	.	.	.	.	.	.	.	.	.	.	X	.	.	X	X	X	.	.	X	.
24	.	.	.	.	.	.	.	.	.	.	.	.	.	.	.	.	.	.	.	X	.	.	X	X	X	.	.	X
25	.	.	.	.	.	.	.	.	.	.	.	.	.	.	.	.	.	.	.	.	X	.	.	X	X	.	.	.
26	.	.	.	.	.	.	.	.	.	.	.	.	.	.	.	.	.	.	.	.	.	X	.	.	.	X	X	.
27	.	.	.	.	.	.	.	.	.	.	.	.	.	.	.	.	.	.	.	.	.	.	X	.	.	X	X	X
28	.	.	.	.	.	.	.	.	.	.	.	.	.	.	.	.	.	.	.	.	.	.	.	X	.	.	X	X

X represents non.zero value in matrix.
. represents zero value in matrix.

Figure 8 - Pentadiagonal Matrix Resulting from Implicit Pressure Formulation of Two Dimensional Problem

accurate to as many digits as the computer will carry.

To increase the accuracy of the pressure solution, the equations were written in a residual form. To provide additional accuracy, most of the variables were declared double precision in the programming code. On the Colorado School of Mines' DECSystem-10, this results in 15+ decimal digits of accuracy. Even though using double precision adds considerably to the run time, the program was reasonably fast. Runtimes ranged from a few hundredths of a second per timestep for a 1x17 matrix to approximately 5 seconds per timestep for a 17x18 matrix.

Model Verification.

The computer model was verified in single-phase flow for a radial and a fractured case, and was verified in multiphase flow for a fractured case. The following describes the model verification procedure.

Single-Phase Flow.

The literature contains various analytical solutions to the diffusivity equation for different boundary conditions. One such solution is a radial flow system presented by Earlougher, Ramey, Miller, and Mueller (1968). Their results are reported in terms of dimensionless pressures and dimen-

sionless times for a $\sqrt{A}/r_w$ ratio of 2,000. This system was simulated using a quadrant of the total flow system, as shown in Figure 9. It could have been simulated using 0.33-ft. by 0.33-ft. blocks throughout the drainage area. However, this leads to an inordinate number of blocks, and an inordinate amount of computer time. To minimize the number of blocks and still maintain the characteristics of radial flow, the block size is increased logarithmically away from the wellbore. The length of blocks away from the wellbore is defined by the equation:

$$\Delta x_{j+1} = \Delta x_j * K \qquad (14)$$

where K is a constant multiplier. Various multipliers were used to increase the block size. The effect of different values of "K" is presented in Figure 10. If the second block is four times as large as the first block and the third block is four times as large as the second block, etc., the comparative results are not particularly good. It was necessary to use a multiplier of 1.5 to achieve reasonable results. A 1.5 multiplier results in the block sizes shown in Table 1 for a radial system. To compare the dimensionless pressure versus dimensionless time of Earlougher, et al., with this model, it is necessary to correct the model flow rate. Since only a quadrant of the actual

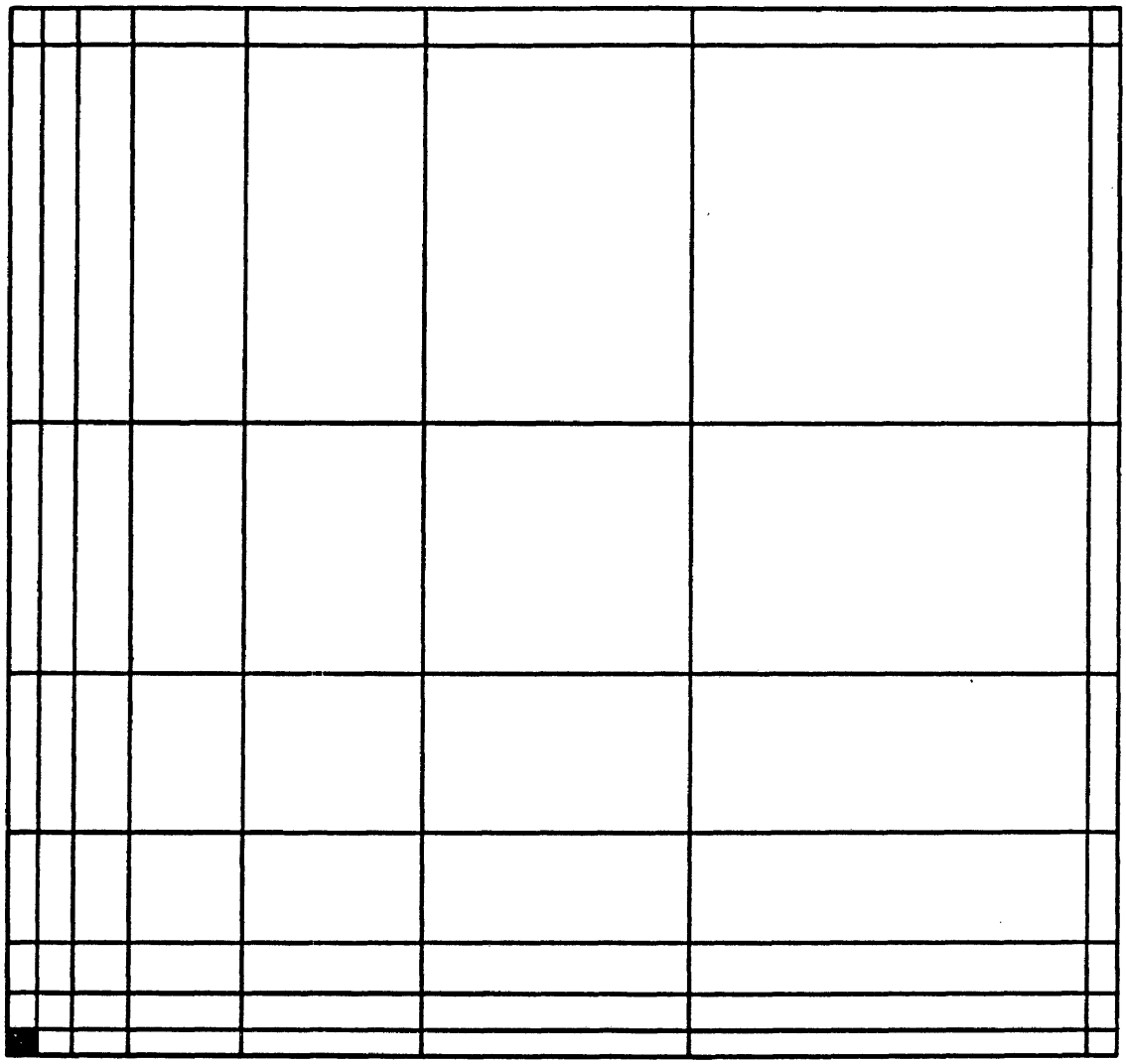

Figure 9. Grid used to simulate radial system.

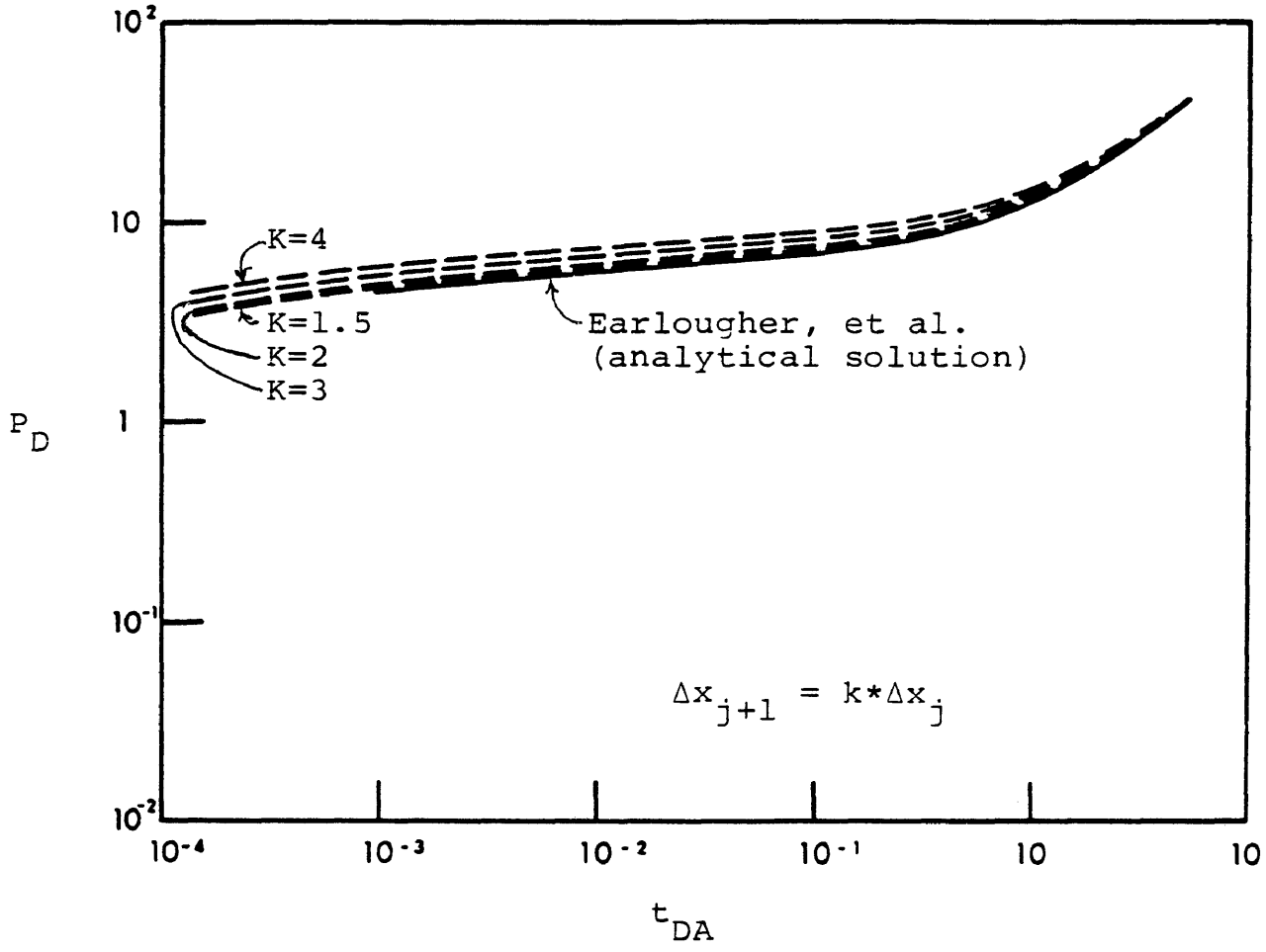

Figure 10 - The effect of various block size multipliers on dimensionless pressure calculated by the computer model.

TABLE 1

Block Sizes for Radial Model
Delta X = Delta Y
r_w = 0.33 ft r_e = 660 ft

Block No.	Size Ft.
1	0.33
2	0.49
3	0.74
4	1.11
5	1.67
6	2.51
7	3.76
8	5.64
9	8.46
10	12.69
11	19.03
12	28.54
13	42.84
14	64.22
15	96.34
16	144.50
17	227.15

flow system is simulated, the model flow rate must be multiplied by four. The equations used to convert the model pressures to dimensionless pressure and the model times to dimensionless time are shown below:

$$P_D = \frac{k\ h\ (P_i - P_{wf})}{141.2\ (\ q_o)(4)} \tag{15}$$

$$t_{DA} = \frac{0.0002637\ k\ 2X_e^{\ 2}}{\phi\ c_t} \left(\frac{k_{ro}}{\mu_o} + \frac{k_{rg}}{\mu_g}\right) t \tag{16}$$

The computer model of the fractured system was validated with Gringarten, Ramey, and Raghavan's (1974) dimensionless pressure versus dimensionless time graphs for an infinite conductivity fracture, since they represent the present industry standard. The fracture system was modeled with the half-fracture length lying along the X axis and the half-fracture width along the Y-axis. Figure 11 shows the geometry used. A fully fractured system results in a linear flow model with the minimum number of blocks. The number of blocks necessary to model the system increases as the fracture length decreases. Table 2 contains the block sizes used to simulate various fracture lengths. The model was run with each of the various fracture lengths and the results were compared to the analytical results derived by

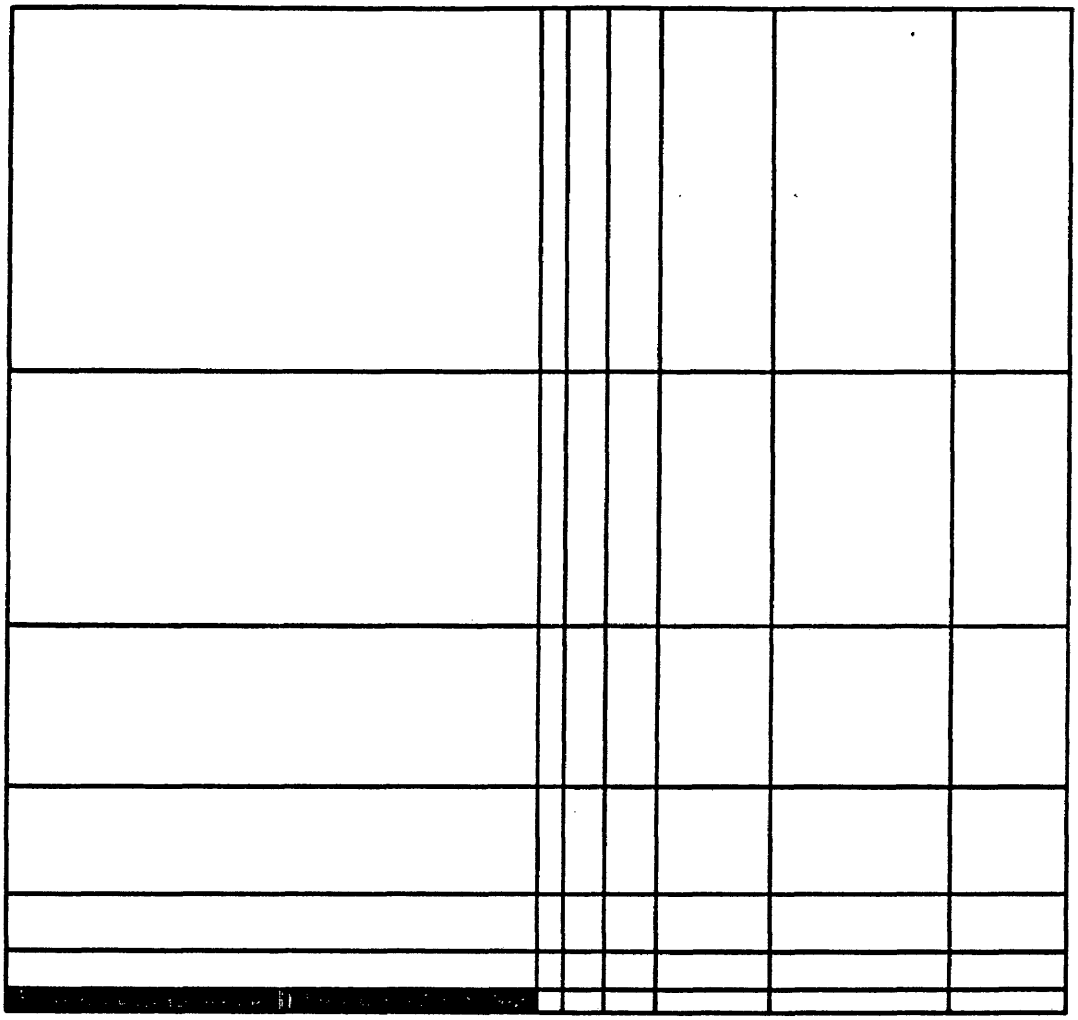

Figure 11. Grid used to simulate fractured system.

TABLE 2

Block Size (feet) in Direction of Fracture for Various Fracture Lengths

Block No.	X_f/X_e 0.2	0.5	1.0
1	132.00	330.00	660.00
2	0.33	0.33	
3	0.50	0.49	
4	0.74	0.74	
5	1.11	1.11	
6	1.67	1.67	
7	2.51	2.51	
8	3.76	3.76	
9	5.64	5.64	
10	8.46	8.46	
11	12.69	12.69	
12	19.03	19.03	
13	28.54	28.54	
14	42.82	42.82	
15	64.22	64.22	
16	96.34	96.34	
17	144.50	41.65	
18	95.14	-	
Total	660.00	660.00	660.00
No. of Blocks	18	17	1

Gringarten, et al. As can be seen in Figures 12 through 14, the model accurately reproduces the analytical solution. The dashed line in these figures represents the simulation results and the solid line represents the analytical results. For the fully fractured case (Figure 13), it is almost impossible to differentiate between the computer solution and the analytical solution. To match the analytical results, it was necessary to begin with extremely small timesteps and increase them logarithmically. The timestep sizes are listed in Table 3. The fluid properties for various assumed compressibilities are shown in Table 4.

Multiphase Flow.

The literature does not contain any analytical solutions for multiphase flow. Therefore, it was necessary to verify the computer model with existing commercially available programs. A commercial model extremely similar to the MUFFS program described by Breitenbach, et al. (1969a,b,c,d) was used for the comparison. An example case was run in which the reservoir pressure started above the bubble point pressure, declined through the bubble point, and continued declining to a low abandonment pressure. The results from this model and from the commercial model agreed within less than one psi throughout the entire run. These results indicate the computer model is working properly.

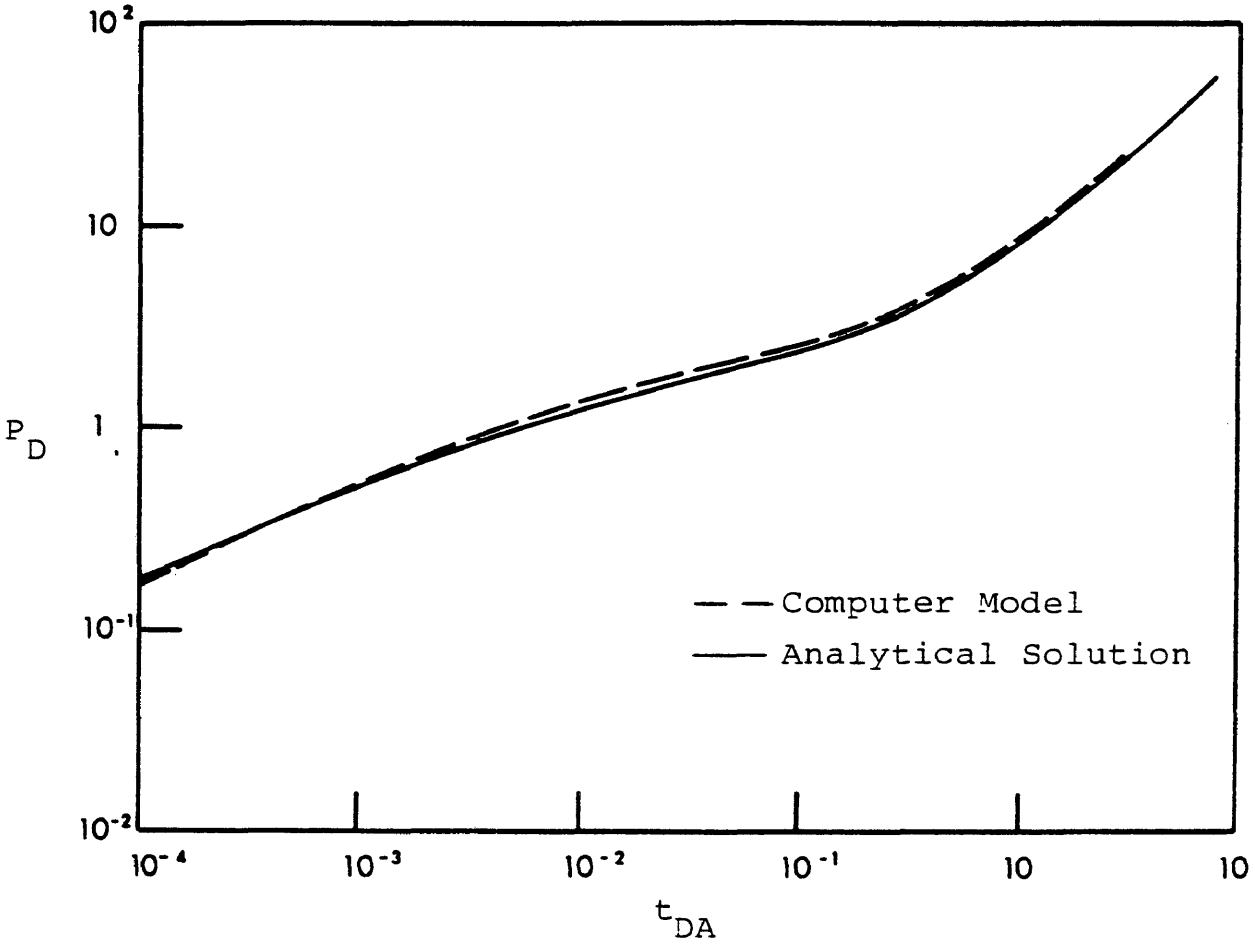

Figure 12 - Comparison of dimensionless pressure calculated by the computer model with the analytical solution of Gringarten, Ramey, and Raghavan (1974) for $X_f/X_e = 0.2$.

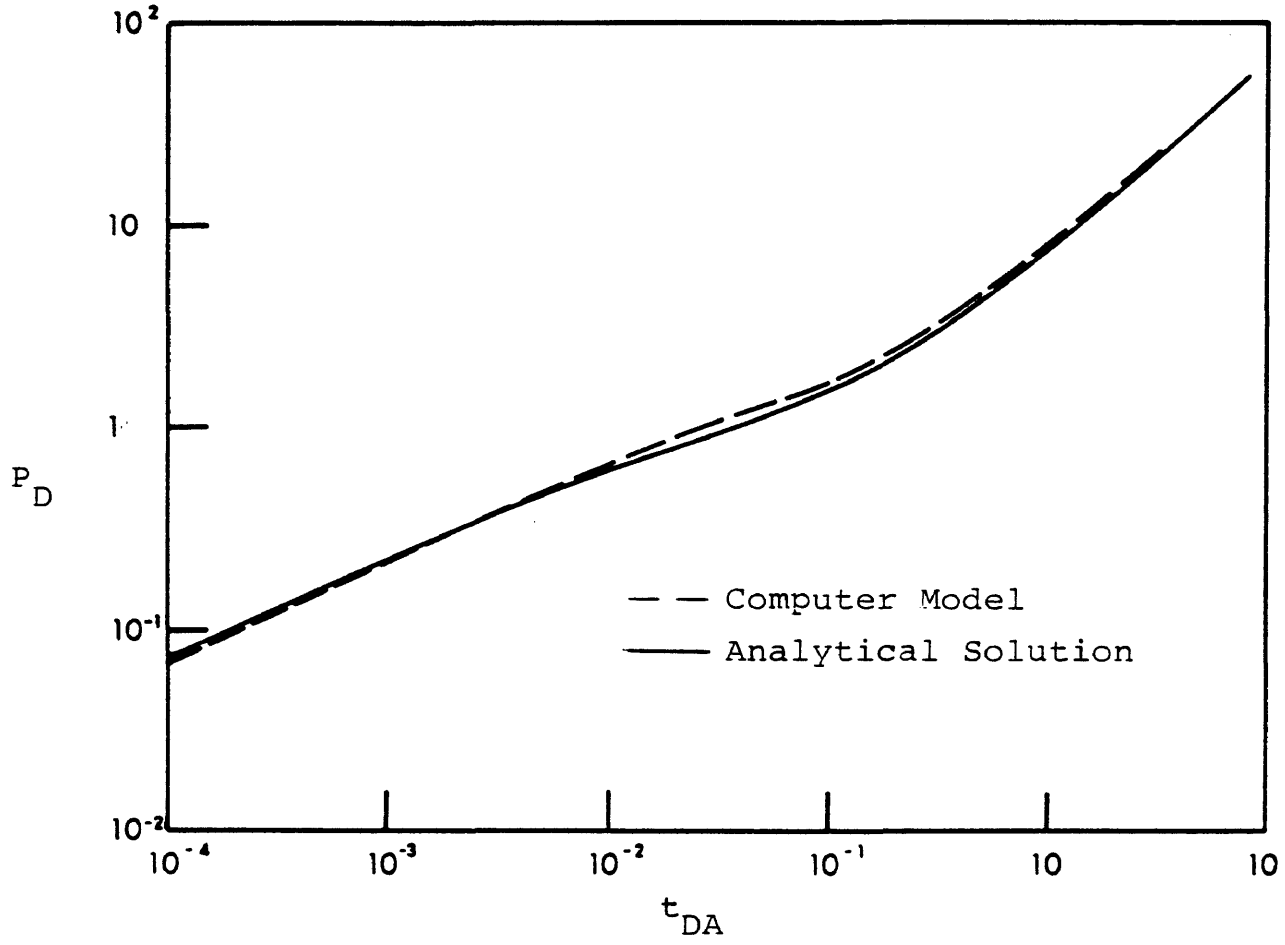

Figure 13 - Comparison of dimensionless pressure calculated by the computer model with the analytical solution of Gringarten, Ramey, and Raghavan (1974) for $X_f/X_e = 0.5$.

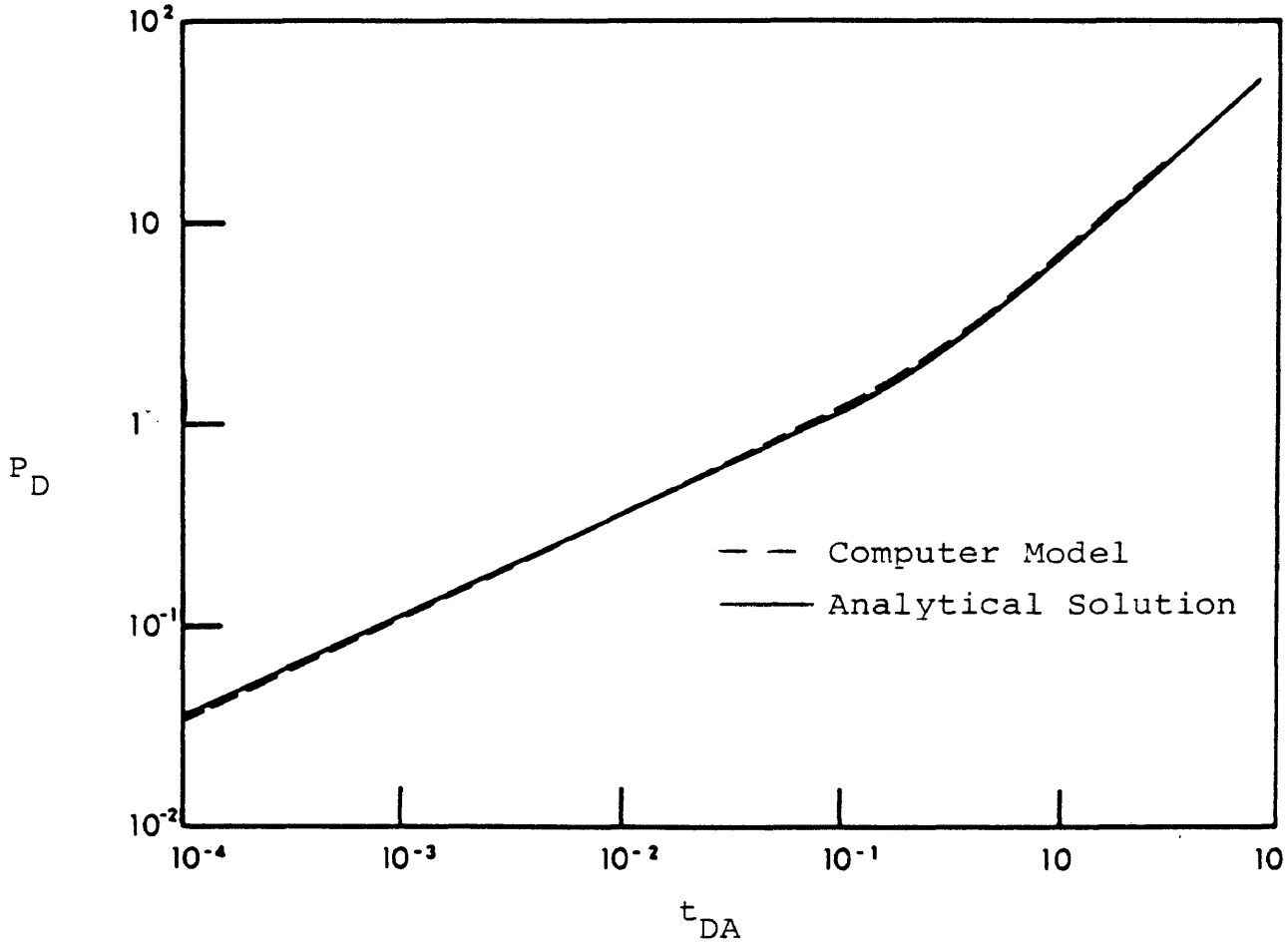

Figure 14 - Comparison of dimensionless pressure calculated by the computer model with the analytical solution of Gringarten, Ramey, and Raghavan (1974) for $X_f/X_e = 1.0$.

TABLE 3

Timestep Sizes for Single-Phase Runs

Number of Timesteps	Size
	Drawdown
5	1 min
5	2
5	5
5	10
5	20
5	40
11	0.5 hr
12	1
24	2
12	4
6	8
7	1 day
7	2
7	4
7	8
14	16
	Buildup
10	1 min
10	2
10	3
12	5
12	10
12	20
12	30
10	1 hr
24	2
18	4
18	8
18	16
18	32
18	64

TABLE 4

Fluid Properties for Single Phase Runs

Compressibility 1/psi	B_o at 100 psia	B_o at 1000 psia
50×10^6	1.046036	1.0
500×10^6	1.580645	1.0
1000×10^6	2.636364	1.0
1500×10^6	5.153846	1.0
2000×10^6	19.000000	1.0

Oil viscosity = 1 cp at all pressures

Of more interest, however, is the computer model's ability to simulate a fractured well in a multiphase system. Raghavan (1977) published the results of simulating a fractured system in multiphase flow. The author contacted Raghavan and he provided the data used in his study. Raghavan's PVT properties are contained in Table 5 and the relative permeability data are shown in Table 6. Other reservoir properties are shown in Table 7. Raghavan's results were published in graphical form as gas-oil ratio versus cumulative production for an absolute permeability of 6.16 md and three fracture lengths: 0.2, 0.5 and 1.0 times X_e. In order to compare the two models' results, it was necessary to digitize his curves. Figure 15 contains a comparison of Raghavan's results with the results of this study. There is good agreement between the two models for the fully fractured case except at large gas-oil ratios. No cases were run at X_f/X_e ratios of 0.2 and 0.5 with permeabilities of 6.16 md because of the computer time which would be required. It is possible the difference in the fully fractured case is caused by differences between the solution techniques and timestep sizes used in the two models. This study used an implicit pressure, explicit saturation model with extremely small-timesteps, whereas Raghavan used a model which "includes implicit rates and

TABLE 5

PVT Properties Obtained from Raghavan

Pressure psi	Formation Volume Factor Oil RB/STB	Gas RCF/SCF	Viscosity Oil cp	Gas cp	Gas In Solution SCF/STB
50	1.0828	.30321	3.06	.0107	60
150	1.0905	.10236	2.998	.0109	99.7
500	1.1180	.02927	2.345	.0114	198
700	1.1340	.01997	2.132	.0118	240
900	1.1495	.01491	1.984	.0123	278
1000	1.1572	.01341	1.930	.0126	297
1200	1.1725	.01051	1.844	.0133	334
1400	1.1880	.00865	1.786	.0141	370
1500	1.1958	.00741	1.7645	.0145	388

TABLE 6

Relative Permeability Data Obtained from Raghavan

Gas Saturation	Oil Relative Permeability	Gas Relative Permeability
0.0	1.0	0.0
0.07	0.62	0.0
0.10	0.51	0.0046
0.15	0.36	0.0170
0.20	0.255	0.036
0.25	0.180	0.056
0.30	0.122	0.082
0.35	0.080	0.118
0.40	0.051	0.16
0.45	0.031	0.21
0.50	0.0198	0.27
0.55	0.0102	0.35
0.69	0.0022	0.69

TABLE 7

Reservoir Properties Used in Raghavan's Model

Porosity	.119
Absolute Permeability, md	6.160
Initial Oil Saturation	1
Initial Pressure, psia	1500
Thickness, ft.	20
X_e, ft.	190
Abandonment Pressure, psi	50
Oil Rate	10 STBOPD per quarter pattern or 40 STBOPD per full pattern

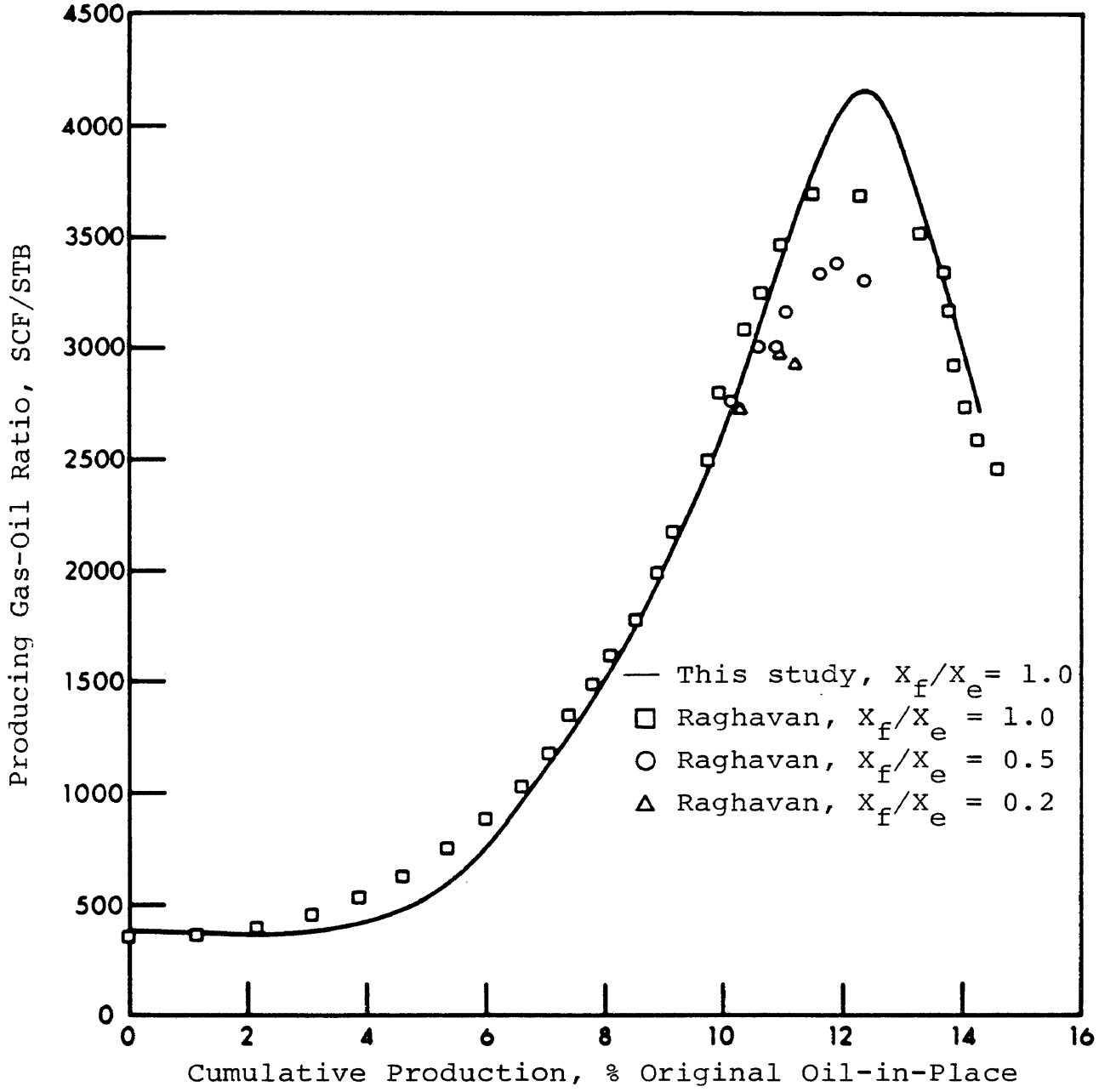

Figure 15 - Comparison of Raghavan's results with the results of this study for a permeability of 6.16 md.

implicit relative permeability calculation procedures" probably with large timesteps. The larger timesteps average the gas-oil ratio changes and much of the detail is lost. Also, the gas-oil ratio from Raghavan's model does not appear to decrease prior to reaching the critical gas saturation as theory predicts it should. Either the drafting is not particularly good or Raghavan's model shows no decrease in the gas-oil ratio until critical gas saturation is reached. This effect may also be a consequence of using a fully implicit scheme with large timesteps instead of an explicit saturation scheme with small timesteps. In spite of the differences in the gas-oil ratio versus cumulative curves, it appears there is a very good match between the results achieved by Raghavan and the results achieved by this model.

Having verified the model in a fully fractured system, it was felt the computer model was sufficiently verified and the remaining fracture length cases were run. Raghavan shows, for 6.16 md, that the gas-oil ratio versus cumulative curves for the three different fracture lengths diverge during the later stages of production. Furthermore, more oil is recovered from a fully fractured reservoir than from a partially fractured reservoir. This effect seems to be permeability and rate dependent. During the verification of

the model in this study, runs were made with lower rates and higher permeabilities than those used by Raghavan. The calculated gas-oil ratio curves for the different fracture penetrations are virtually indistinguishable and there is no difference in the ultimate oil recovery. It appears for any given fracture length, a so-called "critical-rate" exists below which the percentage recovery remains the same and above which ultimate recovery decreases with increasing rate. This would be an extremely interesting area for additional study.

METHOD OF INVESTIGATION AND DATA ANALYSIS

Generation of Data

Seventy different buildup curves were calculated and analyzed. The parameters which were varied included fracture length, absolute permeability, compressibility, drainage area, critical gas saturation, and flow rate. In each case, the production was continued at constant rate until a pressure disturbance occurred at the outer boundary. This assures the well is in pseudo-steady state before it is shut in and the pressure buildup is calculated. The wellbore pressure was then allowed to increase until the pressure was constant throughout the reservoir. The pressure versus time data during the buildup was then plotted as a Horner plot. Three major categories were investigated: single-phase constant-compressibility, single-phase variable-compressibility, and multiphase. Each category is discussed separately.

Single-Phase Constant-Compressibility

Thirty cases were calculated assuming a constant compressibility. The investigated parameters are fracture length (X_f/X_e) and compressibility. The cases were run at compressibilities of 50, 500, 1000, 1500 and 2000 x 10^{-6}

psi^{-1}. Each compressibility was run for fracture penetrations of 0 (radial flow), 0.2, 0.4, 0.6, 0.8, and 1.0 X_f/X_e. In each case the well was produced for 112 days and then shut in and allowed to build up for 96 days. This time schedule assured pressure was the same throughout the reservoir at the end of the build-up. Table 8 shows the case numbers and input data for each case.

Single-Phase Variable-Compressibility

To evaluate the effects of a variable compressibility fluid, five cases were calculated using gas as the producing fluid. The well was produced for 173.1 days and the pressure matrix (and other pertinent data) were saved at 48 days, 98.5 days, 139.1 days, and 173.1 days. At each of these times a restart run was made and the well was allowed to build up for 77.6 days. The pressure versus time data during the buildup was again saved for analysis.

Although the runs assumed a reservoir permeability of 1 md, the drawdowns were so small that these cases were more akin to the constant compressibility cases than a variable compressibility case. The effect of varying compressibility during the buildup should be investigated more thoroughly.

TABLE 8
Parameters for Single Phase Runs

Case No.	Compressibility 1/psi	Dimensionless Fracture Length X_f/X_e
900	50×10^{-6}	0
902	50×10^{-6}	0.2
904	50×10^{-6}	0.4
906	50×10^{-6}	0.6
908	50×10^{-6}	0.8
910	50×10^{-6}	1.0
1000	500×10^{-6}	0
1002	500×10^{-6}	0.2
1004	500×10^{-6}	0.4
1006	500×10^{-6}	0.6
1008	500×10^{-6}	0.8
1010	500×10^{-6}	1.0
1100	1000×10^{-6}	0
1102	1000×10^{-6}	0.2
1104	1000×10^{-6}	0.4
1106	1000×10^{-6}	0.6
1108	1000×10^{-6}	0.8
1110	1000×10^{-6}	1.0
1200	1500×10^{-6}	0
1202	1500×10^{-6}	0.2
1204	1500×10^{-6}	0.4
1206	1500×10^{-6}	0.6
1208	1500×10^{-6}	0.8
1210	1500×10^{-6}	1.0
1300	2000×10^{-6}	0
1302	2000×10^{-6}	0.2
1304	2000×10^{-6}	0.4
1306	2000×10^{-6}	0.6
1308	2000×10^{-6}	0.8
1310	2000×10^{-6}	1.0

Parameters common to all cases:

$k = 100$ md
$X_e = 660$ ft.
$h = 20$ ft.
$\phi = 0.1$
$\mu = 1$ cp.

Multiphase

Thirty-five cases were calculated in which both oil and gas were allowed to flow. Parameters which were varied were average gas saturation at the time of shut in, permeability, fracture length (X_f/X_e), critical gas saturation, flowrate, and drainage area (X_e). The base case assumed a fully fractured reservoir with 100 md permeability and producing at 10 BOPD (per quarter pattern) using Raghavan's PVT rock and reservoir data (as shown in a previous section), and Raghavan's drainage area (3.315 acres for a complete pattern). The only change from Raghavan's data was an increase in the assumed permeability to 100 md. This change was made so larger timestep sizes could be used in the calculations. The effects of fracture peneration were investigated by running cases at dimensionless fracture penetrations (x_f/x_e) of 0.2 and 0.5. The effect of drainage area on the results was analyzed by running a fully fractured case at 40 acres. The effect of flow rate was analyzed by running a case at half the base case flow rate (five barrels per day). The effect of critical gas saturation was studied by changing the critical gas saturation from seven to zero percent of pore volume. In each of these cases the well was produced until the wellbore pressure reached 50 psia. As in the single-phase gas case, the pressure matrix and other

pertinent data were saved at intermediate points: The points chosen represented average gas saturations of one percent, five percent, ten percent, fifteen percent and twenty percent of pore volume. After the drawdown calculation was completed, pressure build-ups were run, beginning at each of the restart points. The pressure buildup was continued until the pressure stabilized throughout the entire reservoir.

Table 9 contains the case numbers and parameters for each run. The rock properties, fluid properties, and other model parameters were the same as those used by Raghavan (1977). See the previous section for specifics of the data. Timestep sizes were 1/2 day until critical gas saturation was reached. They were then decreased until numerical instabilities were eliminated. This process required relatively long computer runs (up to 10 hours of CPU time and 24 hours of elapsed time), but it did have the beneficial effect of eliminating any averaging due to large timesteps, as seen in Raghavan's work. Table 10 contains the timesteps used during the drawdown and buildup in a fully fractured system.

TABLE 9

Parameters for Multiphase Flow Cases

Case No.	Perm md	X_e ft	X_f/X_e	S_{gc}	S_g @ buildup	Flowrate BOPD
101	100	190	1.0	0.07	0.01	40
105	100	190	1.0	0.07	0.05	40
110	100	190	1.0	0.07	0.10	40
115	100	190	1.0	0.07	0.15	40
120	100	190	1.0	0.07	0.20	40
201	100	190	0.5	0.07	0.01	40
205	100	190	0.5	0.07	0.05	40
210	100	190	0.5	0.07	0.10	40
215	100	190	0.5	0.07	0.15	40
220	100	190	0.5	0.07	0.20	40
301	100	190	0.2	0.07	0.01	40
305	100	190	0.2	0.07	0.05	40
310	100	190	0.2	0.07	0.10	40
315	100	190	0.2	0.07	0.15	40
320	100	190	0.2	0.07	0.20	40
401	100	660	1.0	0.07	0.01	40
405	100	660	1.0	0.07	0.05	40
410	100	660	1.0	0.07	0.10	40
415	100	660	1.0	0.07	0.15	40
420	100	660	1.0	0.07	0.20	40
501	100	190	1.0	0.00	0.01	40
505	100	190	1.0	0.00	0.05	40
510	100	190	1.0	0.00	0.10	40
515	100	190	1.0	0.00	0.15	40
520	100	190	1.0	0.00	0.20	40
601	100	190	1.0	0.07	0.01	20
605	100	190	1.0	0.07	0.05	20
610	100	190	1.0	0.07	0.10	20
615	100	190	1.0	0.07	0.15	20
620	100	190	1.0	0.07	0.20	20
701	10	190	1.0	0.07	0.01	40
705	10	190	1.0	0.07	0.05	40
710	10	190	1.0	0.07	0.10	40
715	10	190	1.0	0.07	0.15	40
720	10	190	1.0	0.07	0.20	40

TABLE 10

Time-step Sizes Used in Simulating Fully Fractured System with Raghavan's Rock and Fluid Properties

Number of Timesteps	Size		
	Drawdown		
18	0.5	day	1% Gas Saturation
78	0.5		5% Gas Saturation
38	0.5		Critical Sg at wellbore
315	0.1	day	10% Gas Saturation
406	0.1		15% Gas Saturation
340	0.1		20% Gas Saturation
	Buildup		
10	1	min	
10	2		
10	3		
12	5		
12	10		
12	20		
12	30		
10	1	hr	
24	2		

Analysis of Data

In addition to the standard Horner Plot, two other methods were used to analyze the data. These were: first, to plot pressure versus the square root of time, and secondly, to plot the logarithm of pressure versus the logarithm of time. Earlougher (1977), states that the square-root of time versus pressure plot should result in a straight line which can be analyzed to determine the fracture length. Numerous square-root of time plots were made in this study. They all appeared to curve continuously, and it was extremely difficult to select a straight-line portion from the data. Because of the reliability of the Horner plot and the unreliability of the square root of time versus pressure plot, all attempts to use the pressure versus the square root of time were abandoned.

The second method, also referred to as type curve matching, (plotting logarithm of pressure versus logarithm of time and using the overlay technique to evaluate fractured wells) is highly touted in the literature. It is the observation of this study that it is easy to determine the half-slope line characteristic of fractured wells, but it is extremely difficult to use type curve matching to determine fracture penetration and/or permeability. As the build-up continues, the wellbore pressure approaches the average

reservoir pressure and the log-log plot flattens. These characteristics are totally different from the shape of log-log curves derived for pressure drawdown tests. When using type curve matching to analyze a drawdown test, it is possible to determine X_f/X_e from the depletion "stem" followed by the data. In the buildup case it is virtually impossible to match the log-log plot of the build-up with the correct depletion stem on the type curve. Again, since it is shown that the Horner plot is extremely reliable and useful, further attempts to use type curve matching to obtain a quantitative answer were abandoned.

The analysis of the Horner plots was made in the conventional manner. The slope was determined by drawing a line through the points with the maximum slope. An example is shown in Figure 16. Since a large number of data points are plotted, the resulting curve is quite smooth and it appears that a true straight line portion of the curve does not exist. Instead, the data form an "S"-shaped curve with a concave upward section dominated by linear flow in the fracture and a concave downward section dominated by the boundary. The classical slope for a Horner analysis is taken at the inflection point between these two portions of the curve. Naturally, in the unfractured case there was no linear flow region and the straight line portion of the

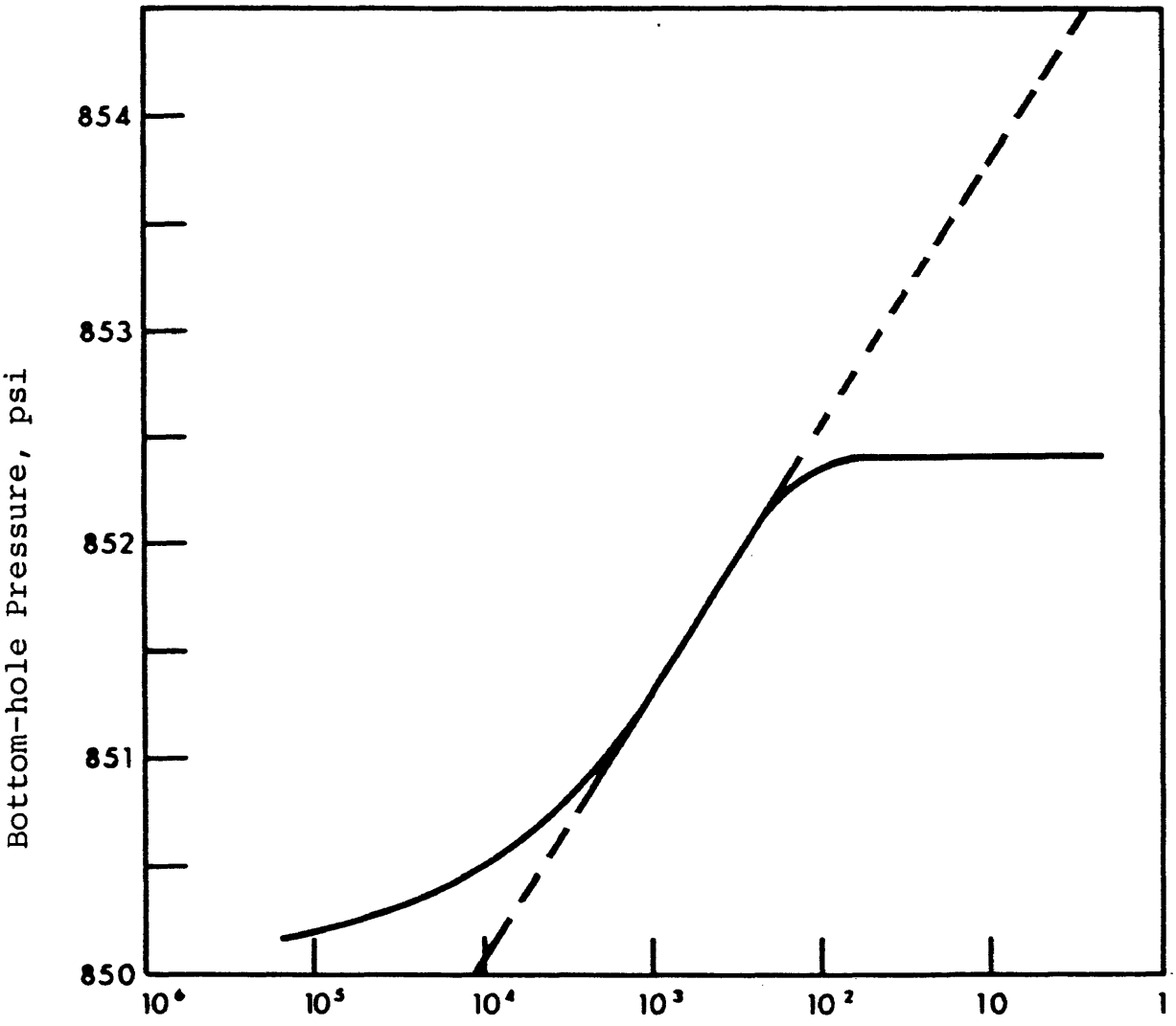

Figure 16 - Horner plot for Case 906 (single phase, flow $X_f/X_e = 0.6$).

curve was very evident. Once the slope had been determined, the Horner time and a pressure are read from the extrapolated straight line. This allows the calculation of P_{1hr}, which is used to calculate the skin factor. These results, along with other pertinent data, were input to a computer program which calculates the apparent permeability to oil (or absolute permeability) and the apparent fracture length.

The permeability to oil was calculated with the equation:

$$k_o = \frac{162.6\ q_o\ \mu_o\ B_o}{mh} . \qquad (17)$$

In single-phase flow, the calculated permeability is the absolute permeability, while in multiphase flow, the calculated permeability is the effective permeability to oil. If the absolute permeability, the average gas saturation in the reservoir at the beginning of the pressure buildup, and the rock properties are known, it is possible to calculate the "true" effective permeability used in the model. For the cases studied, there was not a significant saturation gradient in the reservoir, therefore an average gas saturation approach is acceptable. The effect of a large gas saturation gradient in the reservoir should be investigated in future studies.

The fracture length is calculated from the skin factor. First, the skin factor is calculated from the familiar equation:

$$s = 1.1513 \left[\frac{P_{1hr} - P_{wf}}{m} - \log\left(\frac{k}{\phi\mu c_t r_w^2}\right) + 3.2275\right] . \quad (18)$$

The permeability used in the equation is the known permeability from the model, not the calculated permeability from Equation 17. As will be discussed later, the practical application of the results of this thesis is a trial-and-error method to correct both k and X_f. Therefore, at some time, the actual value of permeability will be known.

In analyzing multiphase flow tests, it is necessary to use total mobility and compressibility to calculate the correct answer. The equation for total mobility is:

$$\left(\frac{k}{\mu}\right)_t = k\left(\frac{k_{ro}}{\mu_o} + \frac{k_{rg}}{\mu_g}\right) . \quad (19)$$

Total compressibility is calculated from the equation

$$c_t = S_o c_o + S_g c_g + c_f. \quad (20)$$

Once the skin factor had been determined, the apparent wellbore radius is calculated from (Earlougher, 1977, p8):

$$r_{wa} = r_w \, e^{-s}. \qquad (21)$$

The apparent fracture length is calculated from the relationship proposed by Prats (1960):

$$X_f = 2 \, r_{wa}.$$

This apparent fracture length is then compared with the known fracture length from the model.

Table 11 contains the results calculated for each case. The case numbers were assigned as follows:

1) Multiphase cases (101-720): The first digit (1-7) is constant for one set of fluid properties or fracture length, etc. The second and third digits are the average gas saturation in the reservoir at shut-in (01 for 1%, etc).
2) Single-phase cases (900-1310): The first digit(s) are the same for a given value of gas compressibility. The last two digits are the fracture penetration (00 is radial, 02 is 20% fracture penetration ratio, etc).

3) Case 20xx is the attempt at variable compressibility. The last two digits indicate that the well was shut in at various times during the drawdown.

The other columns in Table 11 are explained below. k_o-model is the oil permeability at the average gas saturation in the reservoir when the well was shut-in. k_o-calc is the oil permeability calculated from the Horner plot without correction. X_f-model is the fracture length which was input to the model. c_t is the total system compressibility. Skin factor is calculated using the model permeability, a wellbore radius of .33 ft, and is used to calculate X_f-calc. Apparent wellbore radius is calculated assuming a wellbore radius of .33 ft. The remainder of the columns should be self explanatory.

TABLE 11

Results of Pressure Transient Analysis

Case	ko Model md	ko Calc md	k-model/ k-calc	Xf Model ft	Xf calc using k-model ft	Xf calc/ Xf model	Ct 1/psi	Total Mobility md/cp	Press well flowing psi	P1hr psi	Skin Factor	Apparent wellbore radius ft
101	94.46	371.90	0.2540	190.00	37.12	0.1954	162.76E-6	53.22	1448.780	1450.028	-4.030	18.56
105	72.75	289.06	0.2517	190.00	36.23	0.1907	231.31E-6	40.08	1295.040	1296.051	-4.006	18.12
110	51.00	202.50	0.2519	190.00	35.58	0.1873	353.20E-6	62.49	1110.500	1112.064	-3.987	17.79
115	36.00	132.62	0.2715	190.00	43.26	0.2277	603.91E-6	158.89	776.100	778.686	-4.183	21.63
120	25.50	100.86	0.2528	190.00	36.60	0.1927	1994.91E-6	331.21	343.130	346.777	-4.016	18.30
201	94.46	191.38	0.4936	95.00	34.58	0.3640	162.75E-6	53.22	1445.580	1448.225	-3.959	17.29
205	72.75	148.85	0.4887	95.00	33.85	0.3563	231.27E-6	40.08	1290.890	1293.131	-3.937	16.92
210	50.97	103.92	0.4905	95.00	33.94	0.3573	353.54E-6	62.67	1103.840	1107.176	-3.940	16.97
215	36.00	75.12	0.4792	95.00	32.59	0.3430	604.55E-6	158.91	766.000	773.076	-3.899	16.29
220	25.52	52.38	0.4872	95.00	33.36	0.3512	1991.35E-6	330.86	327.460	335.927	-3.923	16.68
301	94.52	115.44	0.8188	38.00	26.37	0.6940	162.52E-6	53.26	1440.030	1445.825	-3.688	13.19
305	72.80	87.40	0.8330	38.00	22.87	0.6018	231.00E-6	40.11	1283.610	1290.147	-3.545	11.43
310	51.04	64.28	0.7940	38.00	21.84	0.5747	353.14E-6	62.39	1093.180	1102.804	-3.499	10.92
315	36.06	44.91	0.8029	38.00	22.30	0.5868	603.17E-6	158.50	750.170	767.626	-3.520	11.15
320	25.61	31.88	0.8031	38.00	21.83	0.5744	1975.34E-6	329.44	300.360	325.118	-3.499	10.91
401	94.52	366.35	0.2580	660.00	128.46	0.1946	162.52E-6	53.26	1449.050	1448.293	-5.271	64.23
405	72.80	286.67	0.2540	660.00	127.09	0.1926	231.09E-6	40.11	1295.550	1293.923	-5.260	63.54
410	51.04	202.48	0.2521	660.00	123.56	0.1872	352.73E-6	62.39	1111.320	1109.078	-5.232	61.78
415	36.06	142.81	0.2525	660.00	124.23	0.1882	602.20E-6	158.48	777.710	775.191	-5.238	62.11
420	25.61	104.11	0.2452	660.00	119.17	0.1806	1979.80E-6	329.47	345.830	340.160	-5.196	59.58

TABLE 11

(Continued)

Case	ko Model md	ko Calc md	k-model/ k-calc	Xf Model ft	Xf calc using k-model ft	Xf calc/ Xf model	Ct 1/psi	Total Mobility md/cp	Press well flowing psi	Plhr psi	Skin Factor	Apparent wellbore radius ft
501	94.46	369.53	0.2556	190.00	36.89	0.1942	163.24E-6	56.50	1447.450	1448.762	-4.024	18.45
505	71.66	282.90	0.2533	190.00	36.45	0.1918	243.15E-6	56.97	1262.400	1263.747	-4.011	18.22
510	49.56	192.63	0.2573	190.00	36.83	0.1938	405.13E-6	71.40	1027.460	1029.008	-4.022	18.41
515	34.91	135.73	0.2572	190.00	37.44	0.1971	749.26E-6	177.28	684.620	687.675	-4.038	18.72
520	25.02	99.30	0.2520	190.00	37.92	0.1996	2409.68E-6	344.53	284.690	287.596	-4.051	18.96
601	94.46	373.10	0.2532	190.00	36.24	0.1907	162.72E-6	53.23	1450.540	1451.181	-4.006	18.12
605	74.11	294.45	0.2517	190.00	36.28	0.1910	226.79E-6	40.88	1305.870	1306.385	-4.007	18.14
610	52.03	199.11	0.2613	190.00	38.21	0.2011	343.71E-6	59.71	1127.580	1128.249	-4.059	19.11
615	37.11	146.23	0.2538	190.00	36.29	0.1910	570.65E-6	151.15	811.760	813.326	-4.007	18.15
620	26.32	104.08	0.2529	190.00	36.13	0.1901	1810.84E-6	317.24	385.070	386.952	-4.003	18.06
701	9.45	32.03	0.2951	190.00	43.70	0.2300	162.30E-6	5.33	1420.180	1410.173	-4.193	21.85
705	7.29	27.80	0.2620	190.00	37.53	0.1975	230.51E-6	4.02	1257.600	1242.351	-4.041	18.77
710	5.06	18.07	0.2801	190.00	39.14	0.2060	366.87E-6	6.49	1024.010	998.716	-4.083	19.57
715	3.56	13.78	0.2584	190.00	36.98	0.1946	643.74E-6	16.56	648.540	624.544	-4.026	18.49
720	2.55	10.72	0.2380	190.00	35.25	0.1855	2028.94E-6	33.11	194.640	143.486	-3.978	17.62

TABLE 11

(Continued)

Case	ko Model md	ko Calc md	k-model/ k-calc	Xf Model ft	Xf calc using k-model ft	Xf calc/ Xf model	Ct 1/psi	Total Mobility md/cp	Press well flowing psi	Pihr psi	Skin Factor	Apparent wellbore radius ft
900	100.00	96.29	1.0386	0.66	0.74	1.1264	49.26E-6	100.00	832.060	848.865	-0.119	0.37
902	100.00	133.86	0.7470	128.00	76.89	0.6007	49.26E-6	100.00	847.127	849.355	-4.758	38.44
904	100.00	184.54	0.5419	264.00	109.03	0.4130	49.26E-6	100.00	849.035	850.112	-5.107	54.52
906	100.00	264.16	0.3786	396.00	112.47	0.2840	49.26E-6	100.00	850.058	850.777	-5.138	56.23
908	100.00	339.44	0.2946	528.00	121.29	0.2297	49.26E-6	100.00	850.642	851.138	-5.214	60.65
910	100.00	394.18	0.2537	660.00	127.06	0.1925	49.26E-6	100.00	850.851	851.245	-5.260	63.53
1000	100.00	96.29	1.0386	0.66	0.71	1.0689	411.13E-6	100.00	961.880	975.705	-0.067	0.35
1002	100.00	131.92	0.7580	128.00	77.43	0.6049	411.13E-6	100.00	977.027	976.984	-4.765	38.71
1004	100.00	183.00	0.5465	264.00	108.82	0.4122	411.13E-6	100.00	978.941	978.381	-5.105	54.41
1006	100.00	259.35	0.3856	396.00	114.57	0.2893	411.13E-6	100.00	979.968	979.516	-5.157	57.29
1008	100.00	348.47	0.2870	528.00	115.52	0.2188	411.13E-6	100.00	980.557	980.214	-5.165	57.76
1010	100.00	383.56	0.2607	660.00	131.38	0.1991	411.13E-6	100.00	980.787	980.380	-5.294	65.69
1100	100.00	97.20	1.0288	0.66	0.67	1.0202	694.67E-6	100.00	969.039	982.102	-0.020	0.34
1102	100.00	130.35	0.7672	128.00	79.04	0.6175	694.67E-6	100.00	984.242	983.581	-4.785	39.52
1104	100.00	180.97	0.5526	264.00	110.36	0.4180	694.67E-6	100.00	986.158	985.157	-5.119	55.18
1106	100.00	261.01	0.3831	396.00	113.58	0.2868	694.67E-6	100.00	987.186	986.461	-5.148	56.79
1108	100.00	343.72	0.2909	528.00	117.31	0.2222	694.67E-6	100.00	987.775	987.198	-5.180	58.66
1110	100.00	368.88	0.2711	660.00	136.43	0.2067	694.67E-6	100.00	988.005	987.351	-5.331	68.22

TABLE 11

(Continued)

Case	ko Model md	ko Calc md	k-model/ k-calc	Xf Model ft	Xf calc using k-model ft	Xf calc/ Xf model	Ct 1/psi	Total Mobility md/cp	Press well flowing psi	Phr psi	Skin Factor	Apparent wellbore radius ft
1200	100.00	97.34	1.0273	0.66	0.65	0.9871	902.03E-6	100.00	971.401	984.159	0.013	0.33
1202	100.00	128.81	0.7763	128.00	79.74	0.6230	902.03E-6	100.00	986.645	985.669	-4.794	39.87
1204	100.00	179.00	0.5587	264.00	111.40	0.4220	902.03E-6	100.00	988.563	987.329	-5.129	55.70
1206	100.00	251.32	0.3932	396.00	116.56	0.2944	902.03E-6	100.00	989.592	988.673	-5.174	58.28
1208	100.00	343.72	0.2909	528.00	115.33	0.2184	902.03E-6	100.00	990.181	989.510	-5.163	57.66
1210	100.00	373.08	0.2680	660.00	134.56	0.2039	902.03E-6	100.00	990.411	989.675	-5.318	67.28
1300	100.00	97.49	1.0258	0.66	0.64	0.9764	1060.29E-6	100.00	972.571	985.107	0.024	0.32
1302	100.00	126.13	0.7928	128.00	82.73	0.6464	1060.29E-6	100.00	987.846	986.583	-4.831	41.37
1304	100.00	178.02	0.5617	264.00	111.78	0.4234	1060.29E-6	100.00	989.765	988.390	-5.132	55.89
1306	100.00	250.43	0.3993	396.00	120.79	0.3050	1060.29E-6	100.00	990.795	989.729	-5.210	60.40
1308	100.00	331.54	0.3016	528.00	122.11	0.2313	1060.29E-6	100.00	991.384	990.570	-5.220	61.05
1310	100.00	366.81	0.2726	660.00	137.04	0.2076	1060.29E-6	100.00	991.614	990.788	-5.336	68.52
2001	1.00	3.73	0.2681	190.00	38.65	0.2034	757.17E-6	1.00	1484.389	1484.530	-4.070	19.33
2005	1.00	3.88	0.2574	190.00	37.24	0.1960	785.79E-6	1.00	1431.810	1431.984	-4.033	18.62
2010	1.00	3.96	0.2527	190.00	36.28	0.1909	828.31E-6	1.00	1363.466	1363.646	-4.007	18.14
2015	1.00	3.92	0.2549	190.00	36.67	0.1930	861.89E-6	1.00	1308.186	1308.317	-4.018	18.34
2020	1.00	3.97	0.2519	190.00	36.30	0.1911	892.69E-6	1.00	1261.590	1261.710	-4.007	18.15

RESULTS

The results of this investigation are summarized in two graphs, Figures 17 and 18. The first of these is a plot of model permeability divided by the permeability calculated from the Horner plot versus the actual fracture penetration ratio. The small circles on Figures 17 and 18 are data points from this study. The large circles show the number of single-phase and multiphase points plotted at the shown value of fracture penetration ratios. The dashed line is the proposed relationship. The two solid lines are the relationships advocated by Russell and Truitt (1964) and Raghavan, Cady, and Ramey (1972). For a fracture penetration ratio of 0, i.e. radial flow, the Horner plot directly yields the correct value of permeability. As the fracture penetration ratio increases, using the uncorrected Horner permeablities can result in calculated permeabilities of up to four times the model permeabilities. This effect was observed by Raghavan, Cady and Ramey's study of the data generated by Russell and Truitt. Their results for Horner plotting are superimposed on Figure 17. It can be seen there is excellent agreement with this study up to fracture penetration ratios of approximately 0.7. For fracture penetration ratios greater than 0.7, Raghavan, Cady and Ramey's

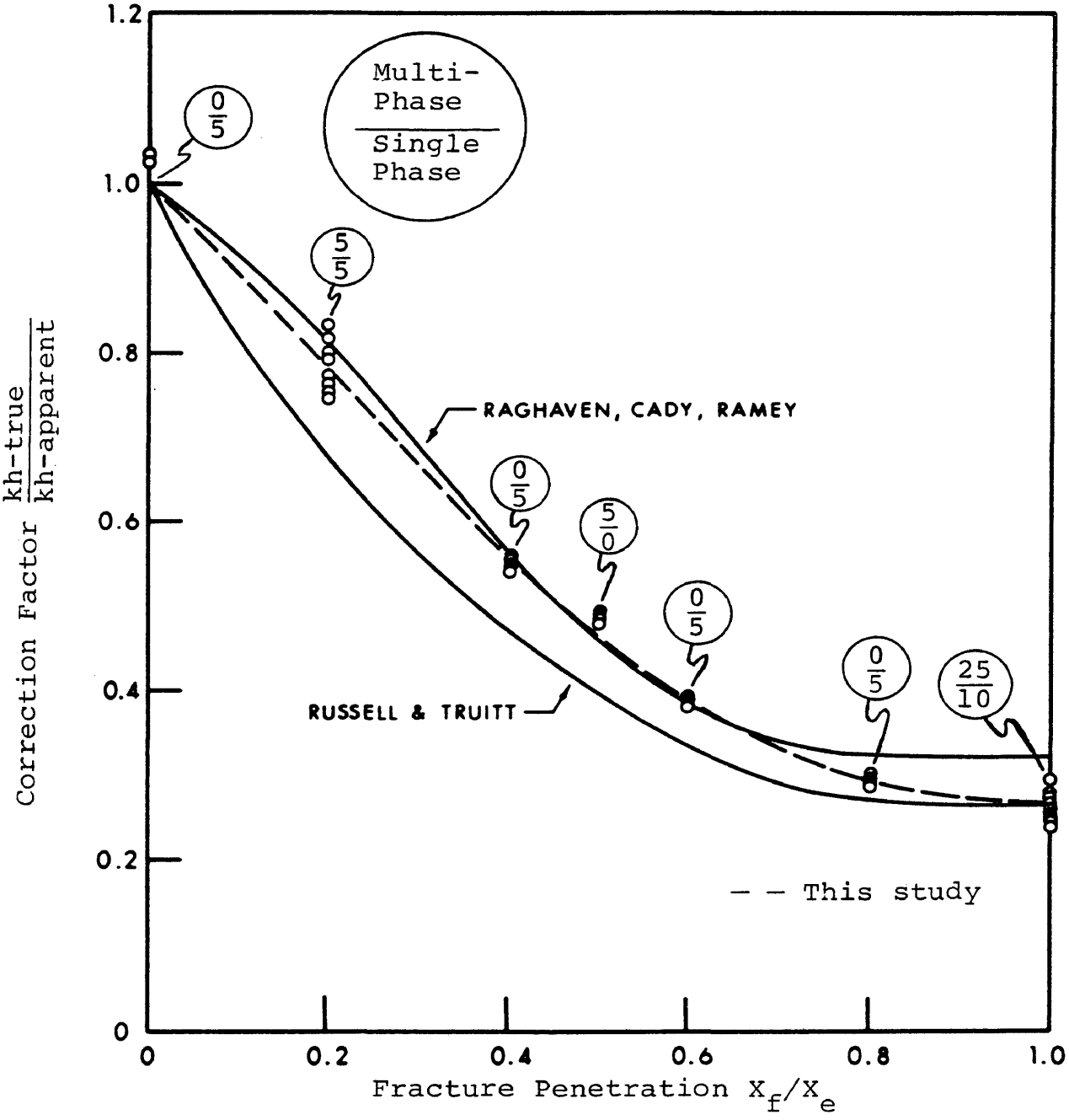

Figure 17 - Comparison of the results from this study with the results of Russell and Truitt, and Raghavan, Cady, and Ramey - kh correction factor.

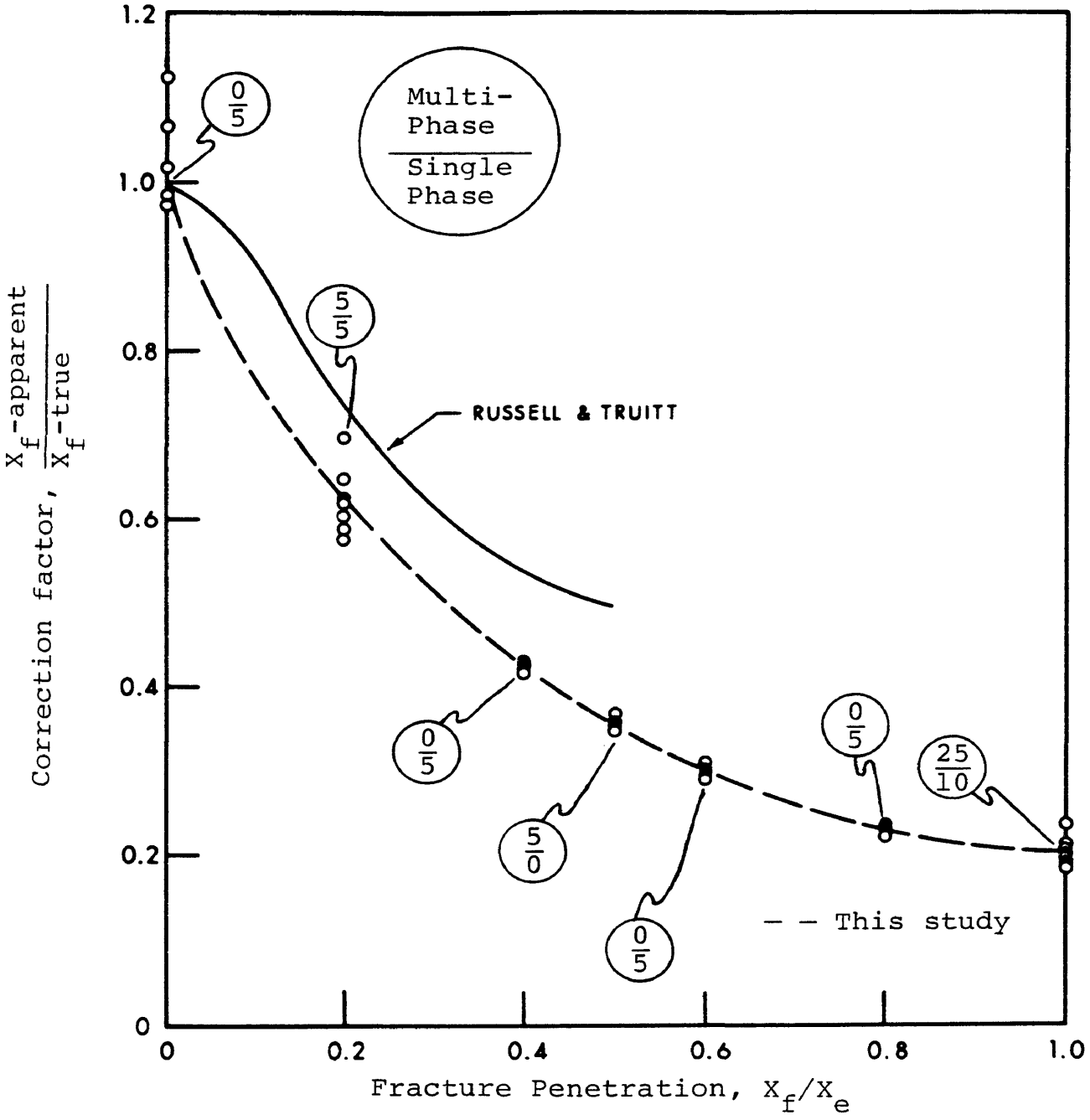

Figure 18 - Comparison of the results from this study with the results of Russell and Truitt - X_f correction factor.

data deviate significantly from the data obtained in this study. This point corresponds with a flattening of Raghavan, Cady and Ramey's curve. Their correlation is based upon one data point at a fracture penetration ratio of one. It is suspected they misplotted or miscalculated this one data point and consequently their correlation flattens in this region.

Until now, many companies have not used build up tests following fracture treatments to calculate fracture penetration. When a fracture penetration is calculated using the uncorrected Horner plot and apparent skin factor, the calculated fracture length is considerably shorter than the fracture length which should have been created by the volume of sand and fluid which was pumped. In analyzing the data from this study, it is determined that the fracture penetration calculated from the Horner plot must be adjusted. The amount of correction is a function of the true fracture penetration ratio. Figure 18 shows the fracture penetration calculated from the Horner plot divided by the model fracture penetration as a function of the model fracture penetration. It can be seen when the well is in radial flow, the Horner plot calculates an extremely good answer for the apparent fracture penetration. As the actual fracture penetration increases, the fracture penetration calculated

from the Horner plot without correction can be as much as five times too short. On Figure 18 the solid line shows Russell and Truitt's results. Raghavan, et al., did not calculate an apparent fracture length in their study. Surprisingly, Russell and Truitt's results vary considerably from those of this study, even though the general trend is the same.

It is necessary to perform a trial and error calculation to determine the true fracture penetration. Example calculations of this trial-and-error solution are contained in the next section.

PRACTICAL APPLICATION OF RESULTS WITH EXAMPLES

EXAMPLE 1 - Single-Phase Flow.

Case 906 is used to demonstrate the application of the described technique to a single-phase case. Figure 16 contains the Horner plot. The solution method is trial and error using successive substitution.

Known:

Oil Well	
Flowrate	40 STBOPD
X_e	660 ft.
h	20 ft.
ϕ	0.10
$\overline{P}$	852.40 psi
P_{1hr}	850.777 psi
P_{wf}	850.058 psi
c_t	49.26×10^{-6} psi^{-1}
μ_o	1 cp
B_o	1.00725 RB/STB
m	1.24 psi/cycle

The pressure dependent variables (B_o, μ_o, and c_t) were all determined at average reservoir pressure. This may not be the best pressure to use to determine these parameters,

but, in this example, the pressure drawdown is so small that there is no difference between using average pressure and using the wellbore pressure.

The solution technique consists of guessing X_f and then calculating k and X_f. This process is continued until the assumed and calculated values of X_f are in agreement.

Step 1 - Calculate apparent permeability from Horner plot (k_{BU}).

$$k_{BU} = \frac{162.6\ q\ \mu\ B}{mh}$$

$$= \frac{(162.6)(40)(1)(1.00725)}{(1.24)(20)}$$

$$= 264.16 \text{ md.}$$

Step 2 - Assume $X_f = 0$ and calculate k and X_f.

a) Calculate k

At $X_f/X_e = 0$, $k/k_{BU} = 1$ (from Figure 17).

$k = k_{BU} * (k/k_{BU})$

$= 264.16 * 1$

$= 264.16$

b) Calculate skin factor using k from Step 2-a.

$$s = 1.1513 \left\{\frac{P_{1hr} - P_{wf}}{m} - \log\left(\frac{k}{\mu\, c_t\, \phi\, r_w^2}\right) + 3.2275\right\}$$

$$= 1.1513 \left\{\frac{850.777 - 850.058}{1.24}\right.$$

$$\left. -\log\left[\frac{264.16}{(1)(49.26\times10^{-6})(.1)(.33^2)}\right]\right.$$

$$\left. + 3.2275\right\}$$

$$= -5.624$$

c) Calculate the apparent X_f using the value of skin factor from Step 2-b.

$$X_f\text{-apparent} = 2\, r_w\, e^{-S}$$

$$= 2(.33)e^{5.624}$$

$$= 182.8 \text{ ft.}$$

d) The apparent fracture length from Step 2-c must be corrected using the correction factor from Figure 18. Figure 18 is entered with the assumed X_f/X_e ratio from Step 2-a.

At an assumed X_f/X_e ratio of 0 (Step 2-a), X_f-apparent / X_f = 1.

$X_f = X_f\text{-apparent} / (X_f\text{-apparent}/X_f)$

$$= 182.8 / 1$$

$$= 182.8$$

Step 3 - Check to see if X_f-assumed is the same as X_f-calculated in Step 2-d. If so, the value of X_f is the value calculated in Step 2-d and the value of k is the value calculated in Step 2-a. If the assumed and calculated values of X_f are not close enough, guess a new value of X_f and do Step 2 over again.

A reasonable guess for X_f is the value which has just been calculated. Table 12 contains the results of using successive substitution to determine the correct value of k and X_f.

Trial 6 results in essentially the same value for X_f-guessed and X_f-calculated. The value of k from the trial and error procedure is 108 md. The value used in the model to calculate the pressure-time data was 100 md. Therefore the value of k from this procedure is 8 percent high. If no correction factors had been applied, the value of k would have been 164 percent too high.

The value of X_f from the trial and error procedure is 384 ft. This compares with a value of 396 ft which was used in the model. This procedure yields a value of X_f which is 3 percent too low compared to a value which would have been

Table 12

Calculation of Correct k and X_f

for Single-Phase Flow Case

Trial Number	1	2	3	4	5	6
X_f guessed	0	183	290	352	377	383
X_f/X_e guessed	0	.277	.440	.534	.571	580
k/k_{BU} from Fig 17	1	.697	.532	.448	.418	.410
k	264	184	140	118	110	108
s	-5.62	-5.44	-5.31	-5.22	-5.19	-5.18
X_f-apparent	182	152	133	122	118	117
X_f/X_f-apparent from Figure 18	1	.526	.378	.325	.309	.305
X_f calculated	183	290	352	377	383	384

54 percent too low if no correction factor had been applied.

Being within 8 percent on permeability and 3 percent on fracture length is quite good compared to the usual uncertainty encountered in predicting these quantities.

EXAMPLE 2 - Multiphase Flow.

Case 210 is used to demonstrate the application of the technique to multiphase flow. Figure 19 is the Horner plot of the data.

Known:

Oil Well

Flow Rate	40 BOPD
GOR	1077.1 SCF/STB
Average Gas Saturation	10 percent
X_e	190 ft.
h	20 ft.
ϕ	0.119
$\bar{P}$	1116.57 psi
P_{wf}	1103.84 psi
P_{1hr}	1107.176 psi
m	6.860 psi/cycle
c_t @ $\bar{P}$	353.54×10^{-6} psi^{-1}
μ_o @ $\bar{P}$	1.878 cp

μ_g @ $\bar{P}$	0.0131 cp
k_{ro}	0.51
k_{rg}	0.00477
B_o	1.1661 RB/STB
B_g	0.01172 RCF/SCF
R_s	267 SCF/STB

The pressure dependent variables are determined at the average reservoir pressure, and the saturation dependent variables are determined at the average saturation. Again, as stated in Example 1, the average pressure and saturation may not be the best values to use to determine these parameters if the well has a large drawdown.

Fracture length and total mobility are calculated without knowing relative permeability. However, to calculate absolute permeability, relative permeabilities must be known.

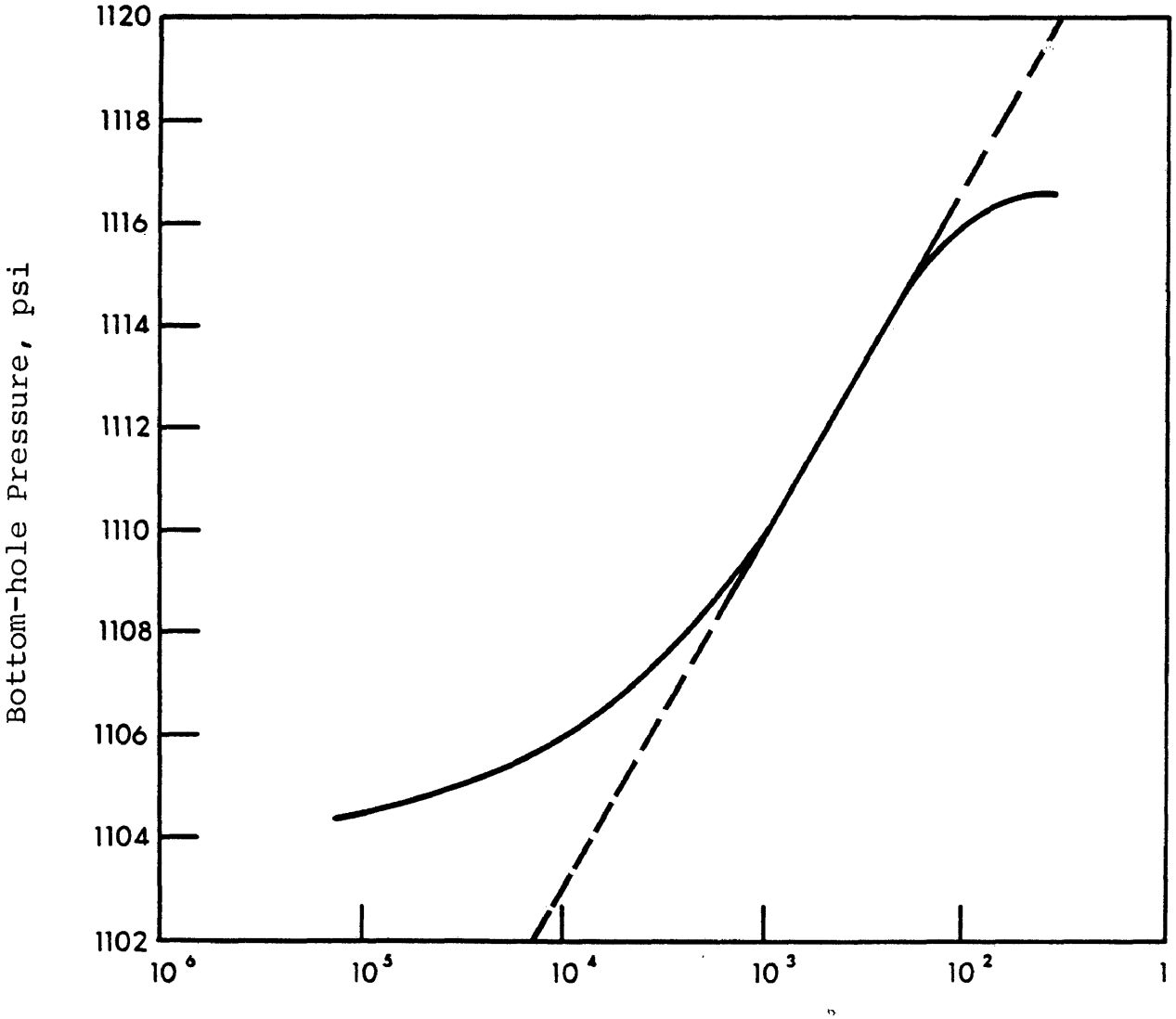

Figure 19 - Horner plot for Case 210 (multiphase flow, S_g = 10%, X_f/X_e = 0.5).

Step 1 - Calculate apparent total mobility from Horner plot, $(k/\mu)_{BU}$.

$$q_{res} = q_o B_o + q_o (R-R_s) B_g/5.615$$
$$= (40)(1.1661)$$
$$+ (40)(1077.1-267)(.01172)/5.615$$
$$= 114.28 \text{ BPD}$$

$$\left(\frac{k}{\mu}\right)_t = \frac{162.6\ q_{res}}{mh}$$

$$= \frac{(162.6)(114.28)}{(6.860)(20)}$$

$$= 135.44.$$

Step 2 - Assume $X_f = 0$ and calculate $(k/\mu)_t$ and X_f.

a) Calculate k/ μ

At $X_f/X_e = 0$, $(k/\mu)/(k/\mu)_{BU} = 1.0$ (from Figure 17).

$(k/\mu) = (k/\mu) / [(k/\mu)//)k/\mu)_{BU}]$

$= 135.44 / 1.0$

$= 135.44$

b) Calculate skin factor using k/μ from Step 2-a.

$$s = 1.1513 \left\{\frac{P_{1hr} - P_{wf}}{m} - \log\left(\frac{(k/\mu)_t}{c_t\ \phi\ r_w^2}\right)\right.$$

$$+ 3.2275\}$$

$$= 1.1513 \left\{\frac{1107.176 - 1103.84}{6.86}\right.$$

$$\left. -\log \left(\frac{161.85}{(353.54 \times 10^{-6})(.119)(.33^2)}\right)\right.$$

$$+ 3.2275\}$$

$$= -4.414$$

c) Calculate the apparent X_f using the value of skin factor from Step 2-b.

$$X_f\text{-apparent} = 2r_w e^{-s}$$

$$= 2(.33)e^{4.414}$$

$$= 54.54 \text{ ft}$$

d) The apparent fracture length from Step 2-c must be corrected using the correction factor from Figure 18. Figure 18 is entered with the assumed X_f/X_e ratio from Step 2-a.

At an assumed X_f/X_e ratio of 0 (Step 2-a), X_f/X_e-apparent = 1.0

$X_f = X_f\text{-apparent} / (X_f\text{-apparent}/X_f)$

$= 54.54 / 1.0$

$= 54.54$

Step 3 - Check to see if X_f-assumed is the same as X_f-calculated in Step 2-d. If so, the value of X_f is the value calculated in Step 2-d and the value of k/μ is the value calculated in Step 2-a. If the assumed and calculated values of X_f are not close enough, guess a new value of X_f and do Step 2 over again.

A reasonable guess for X_f is the value which has just been calculated. Table 13 contains the results of using successive substitution to determine the correct value of k/μ and X_f.

Trial 6 results in essentially the same value for X_f-guessed and X_f-calculated. The value of X_f from the trial and error procedure is 103 ft. This compares with a value of 95 ft which was used in the model. This procedure yields a value of X_f which is 8 percent too high compared to a value which would have been 47 percent too low if no correction factor had been applied.

The value of $(k/\mu)_t$ from the trial and error procedure is 60 md. Effective permeability to oil and to gas can be calculated by assuming each phase flows independently.

Table 13

Calculation of Correct k/μ and X_f

for Multiphase Flow Case

Trial Number	1	2	3	4	5	6
X_f guessed	0	50	78	93	100	102
X_f/X_e guessed	0	.263	.408	.491	.527	.539
$(k/\mu)/(k\ \mu_{BU})$ from Figure 17	1	.713	.562	.485	.453	.443
$(k/\mu)_t$	135	97	76	66	61	60
s	-4.33	-4.16	-4.04	-3.96	-3.93	-3.92
X_f-apparent	50	42	37	35	34	33
X_f/X_f-apparent from Figure 18	1	.543	.401	.347	.328	.322
X_f	50	78	93	100	102	103

For oil:

$$k_o = \frac{162.6\ q_o\ \mu_o\ B_o}{mh} * \left(\frac{k}{k_{BU}}\right)$$

$$= \frac{162.6\ (40)(1.878)(1.1661)}{6.860\quad 20} * .443$$

$$= 46.0 \text{ md}$$

From k_o and k_{ro}:

$$k = \frac{k_o}{k_{ro}}$$

$$= \frac{46.0}{.51}$$

= 90.2 md compared to 100 md from the model.

For gas:

$$k_g = \frac{162.6\ q_g\ \mu_g\ B_g}{mk} *\left(\frac{k}{k_{BU}}\right)$$

$$= \frac{162.6(40)(1077-267)(.013)(.01172)/5.615}{6.860\quad 20} * .443$$

= .46 md.

From k_g and k_{rg}:

$$k = \frac{k_g}{k_{rg}}$$

$$= \frac{.46}{.00477}$$

= 96.8 md compared to 100 md from the model.

The calculated permeability is 10 percent low using oil production data and 3 percent low using gas production data. If the correction procedure had not been followed, the calculated total mobility would have been 82 percent high.

CONCLUSIONS

1) The Horner Plot can be used to reliably calculate both permeability and fracture penetration ratio in a fractured well, provided a correction procedure is used.

2) The same technique can be used for both multiphase flow and single-phase flow, provided that total mobility and total compressibility are used in the appropriate places.

3) The technique is valid for any drainage area, flow rate, gas saturation, or rock properties, provided the well was producing under pseudo-steady state conditions prior to shut in.

4) The technique in this thesis (correcting the Horner plot) is much easier to apply than either the square-root of time or the log-log technique.

SUGGESTIONS FOR FUTURE RESEARCH

Although the technique described in this thesis appears to be applicable to most of the producing wells in the world, there are still a number of areas which need to be investigated more throughly. These include:

1) It should be possible to derive the mathematics to verify that using radial flow solutions to the diffusivity equation in a linear flow system results in a k-apparent to k-true ratio of 0.25 and an x_f-true to x_f-apparent ratio of 0.2.

2) The effect of finite fracture conductivities should be investigated.

3) The effect of shutting in the well before pseudo-steady state is reached should be investigated.

4) The effect of shutting in the well while the area near the wellbore is below the bubble-point pressure and the area far away from the wellbore is above the bubble point pressure should be investigated. This problem could be coupled with a change in the bubble-

point pressure of the fluids in the near well region because of gas flow.

5) The effect of large pressure drawdowns with a variable compressibility fluid should be investigated.

6) More work should be done to determine if a "critical rate" exists for each fracture length and permeability, above which ultimate recovery is reduced.

7) The shut-in time necessary to obtain the "straight line" region on the Horner plot should be investigated to determine if the equations proposed by Miller, Dyes, and Hutchinson (1950) are valid for fractured wells.

8) Methods to analyze the drawdown portion of the pressure transient curve should be investigated.

9) The use of oil "pseudo-potential" to analyze both the pressure drawdown and the pressure buildup should be investigated

The successful study of items 2 through 6 probably depends upon the creation of a fully implicit simulator so that reasonably sized timesteps can be used. It is possible that this simulator might use the Jacobian Matrix Technique.

NOMENCLATURE

English

a	-	Dimensionless fracture flow capacity.
A	-	Area.
B	-	Formation volume factor.
B_g	-	Gas formation volume factor, RCF/SCF.
B_L	-	Liquid formation volume factor, RCF/SCF.
B_o	-	Oil formation volume factor, RB/STB.
c	-	Compressibility, 1/psi.
c_f	-	Pore volume compressibility, 1/psi.
c_g	-	Gas compressibility, 1/psi.
c_o	-	Oil compressibility, 1/psi.
c_t	-	Total compressibility, 1/psi.
c_{ti}	-	Initial total compressibility, 1/psi.
h	-	Height, ft.
k	-	Absolute permeability, md.
k_f	-	Fracture permeability, md.
k_g	-	Effective permeability to gas, md.
k_o	-	Effective permeability to oil, md.
k_{rg}	-	Relative permeability to gas, md.
k_{ro}	-	Relative permeability to oil, md.
k_t	-	Total permeability, md.
K	-	An arbitrary constant.

m - Slope of Horner plot, psi/cycle.

$m(P)$ - Oil pseudo-potential, md/cp.

P - Pressure, psi.

P_e - Pressure at external boundary, psi.

P_D - Dimensionless pressure, $\frac{kh\ (P_i - P_{wf})}{141.2\ q\ \mu\ B}$

P_i - Initial pressure, psi.

P^* - Pressure obtained from extrapolating Horner plot to $[(t + \Delta t)/\Delta t] = 1$.

$\overline{P}$ - Average reservoir pressure, psi.

P_{wf} - Wellbore flowing pressure, psi.

P_b - Bubble point pressure, psi.

P_f - Wellbore flowing pressure, psi.

P_{1hr} - Pressure on back-extrapolated straight-line portion of semilog plot 1 hour after beginning a transient test, psi.

q - Surface flowrate.

q_g - Surface gas flowrate, MSCFPD.

q_L - Surface liquid flowrate, STBPD.

q_o - Surface oil flowrate, STBPD.

R - Producing gas-oil ratio, SCF/STB.

R_s - Solution gas-oil ratio, SCF/STB.

r_e - Radius of external boundary, ft.

r_w - Radius of wellbore, ft.

r_{wa} - Apparent wellbore radius, ft.

s - Skin factor.

s' - Pseudo-skin factor resulting from fracture and gas saturation around wellbore.

S_g - Gas saturation, fraction.

S_o - Oil saturation, fraction.

t - Flow time.

t_D - Dimensionless time, $\frac{0.0002637\ k\ t}{\phi\ \mu\ c_t\ r_w^2}$

t_{DA} - Dimensionless time based on areas, $\frac{0.0002637\ k\ t}{\phi\ \mu\ c_t\ A}$

t_{DXf} - Dimensionless time based on fracture length, $\frac{0.0002637\ k\ t}{\phi\ \mu\ c_t\ X_f^2}$

W_f - Fracture width, ft.

X_f - Fracture half-length, ft.

X_e - Distance from a centered well to the edge of a square drainage region.

Greek

γ_g - Specific weight of gas.

γ_L - Specific weight of liquid.

γ_t - Specific weight of mixture.

ΔX - Size of cell in X direction.

ΔY - Size of cell in Y direction.

Δt - Shut in time.

μ_g - Gas viscosity, cp.

μ_L - Liquid viscosity, cp.

μ_o - Oil viscosity, cp.

μ_{oi} - Initial oil viscosity, cp.

μ_t - Total viscosity, cp.

π - 3.14159...

ϕ - Porosity, fraction.

REFERENCES

Aziz, Khalid, and Settari, Antonin, 1979, Petroleum Reservoir Simulation: London, Applied Sciences Publishers, LTD.

Breitenbach, E.A., Thurnau, D.H., and van Poollen, H.K., 1968a, Immiscible Fluid Flow Simulator: Society of Petroleum Engineers of AIME, Dallas Meeting (April 22-23, 1968), Preprint No. SPE 2019.

_____ 1968b, The Fluid Flow Simulation Equations: Society of Petroleum Engineers of AIME, Dallas Meeting (April 22-23, 1968), Preprint No. SPE 2020.

_____ 1968c, Solution of the Immiscible Fluid Flow Simulation Equations: Society of Petroleum Engineers of AIME, Dallas Meeting (April 22-23, 1968), Preprint No. SPE 2021.

_____ 1968d, Treatment of Individual Wells and Grids in Reservoir Modeling: Society of Petroleum Engineers of AIME, Dallas Meeting (April 22-23, 1968), Preprint No. SPE 2022.

Earlougher, R.C., Jr., Miller, F.G., and Mueller, T.D., 1967, Pressure Buildup Behavior in a Two-Well Gas-Oil System: Soc. Pet. Eng. J. (June 1967); Trans., AIME 240, p. 195-204.

Earlougher, Robert C., Jr., Ramey, H.J., Jr., Miller, F.G., and Mueller, T.D., 1968, Pressure Distributions in Rectangular Reservoirs: J. Pet. Tech. (Feb. 1968); Trans., AIME 243, p. 199-208.

Evinger, H.H., and Muskat, M., 1941, Calculation of Theoretical Productivity Factor: Trans., AIME, V. 146, p. 126-139.

Fetkovich, M.J., 1973, The Isochronal Testing of Oil Wells: paper SPE 4529 presented at the SPE-AIME 48th Annual Fall Meeting, Las Vegas, Sept. 30-Oct. 3, 1973.

Gringarten, Alain C., Ramey, Henry J., Jr., and Raghavan, R., 1972, Pressure Analysis for Fractured Wells: paper SPE 4051 presented at the SPE-AIME 47th Annual Fall Meeting, San Antonio, Texas, Oct. 8-11, 1972.

_____ 1975, Applied Pressure Analysis for Fractured Wells: J. Pet. Tech. (July 1975); Trans., AIME, V. 259, p. 887-892.

_____ 1974, Unsteady-State Pressure Distributions Created by a Well With a Single Infinite-Conductivity Vertical Fracture: Soc. Pet. Eng. J. (Aug. 1974), p. 347-360.

Horner, D.R., 1951, Pressure Build-Up in Wells: Proc., Third World Pet. Cong., The Hague (1951) Sec. II, p. 503-523.

Letkeman, J.P., and Ridings, R.L., 1970, A Numerical Coning Model: Soc. Pet. Eng. J. (Dec. 1970), p. 418-424.

MacDonald, R.C., and Coats, K.H., 1970, Methods for Numerical Simulation of Water and Gas Coning: Soc. Pet. Eng. J. (Dec. 1970), p. 425-436.

Martin, John C., 1959, Simplified Equations of Flow in Gas Drive Reservoirs and the Theoretical Foundation of Multiphase Pressure Buildup Analyses: Trans., AIME v. 216, p. 309-311.

Matthews, C.S., Brons, F., and Hazebroek, P., 1954, A Method for Determination of Average Pressure in a Bounded Reservoir: Trans., AIME v. 201, p. 182-191.

Miller, C.C., Dyes, A.B., and Hutchinson, C.A., Jr., 1950, The Estimation of Permeability and Reservoir Pressure From Bottom Hole Pressure Build-Up Characteristics: Trans., AIME v. 189, p. 91-104.

Muskat, Morris, 1937, Use of Data on the Build-Up of Bottom-Hole Pressures: Trans., AIME, V. 123, p. 44-48.

Perrine, R.L., 1956, Analysis of Pressure Buildup Curves: Drill and Prod. Prac., API, p. 482-509.

Prats, Michael, and Levine, J.S., 1963, Effect of Vertical Fractures on Reservoir Behavior - Results on Oil and Gas Flow: J. Pet. Tech. (Oct. 1963), p. 1119-1126.

Prats, Michael, Hazebroek, P., and Strickler, W.R., 1962, Effect of Vertical Fractures on Reservoir Behavior - Compressible-Fluid Case: Soc. Pet. Eng. J. (June 1962), p. 87-94.

Prats, Michael, 1961, Effect of Vertical Fractures on Reservoir Behavior - Incompressible Fluid Case: Soc. Pet. Eng. J. (June 1961), p. 103-118.

Raghavan, R., 1976, Well Test Analysis: Wells Producing by Solution Gas Drive: Soc. Pet. Eng. J. (Aug. 1976), Trans., AIME, V. 261, p. 196-208.

_____ 1977, Pressure Transient Analysis of a Vertically Fractured Well Produced by Solution Gas Drive: Soc. Pet. Eng. J. (Oct. 1977), p. 369-376.

Raghavan, R., Cady, Gilbert V., and Ramey, Henry J., Jr., 1972, Well-Test Analysis for Vertically Fractured Wells: J. Pet. Tech. (Aug. 1972); Trans., AIME, V. 253, p. 1014-1020.

Raghavan, R. and Hadinoto, Nico, 1976, Analysis of Pressure Data for Fractured Wells: The Constant Pressure Outer Boundary: paper SPE 6015 presented at the SPE-AIME 51st Annual Fall Technical Conference and Exhibition, New Orleans, Oct. 3-6, 1976.

Ramey, H.J., Jr., and Cobb, William M., 1971, A General Buildup Theory for a Well in a Closed Drainage Area: J. Pet. Tech. (Dec. 1971), p. 1493-1505.

Russell, D.G. and Truitt, N.E., 1964, Transient Pressure Behavior in Vertically Fractured Reservoirs: J. Pet. Tech. (Oct. 1964); Trans., AIME, V. 231, p. 1159-1170.

Scott, J.O., 1963, The Effect of Vertical Fractures on Transient Pressure Behavior of Wells: J. Pet. Tech. (Dec. 1963), p. 1363-1369.

Thurnau, D.H., 1963, Algorithm 195, BANDSOLVE: Communications of the ACM, V. 6, p. 441.

van Everdingen, A.F., 1953, The Skin and Its Influence on the Productive Capacity of a Well: Trans., AIME, V. 198, p. 171-176.

Weller, W.T., 1966, Reservoir Performance During Two-Phase Flow: J. Pet. Tech. (Feb. 1966), p. 240-246.

APPENDIX A

DERIVATION OF THE DIFFUSIVITY EQUATION

The mathematical description of fluid flow in a porous medium is known as the diffusivity equation. It can be derived from three physical principles: (1) The Law of Conservation of Mass; (2) Darcy's Law; and (3) Equation(s) of State. The diffusivity equation will be derived for the following elemental volume which is a rectangular parallelopiped with dimensions Δx, Δy, and Δz.

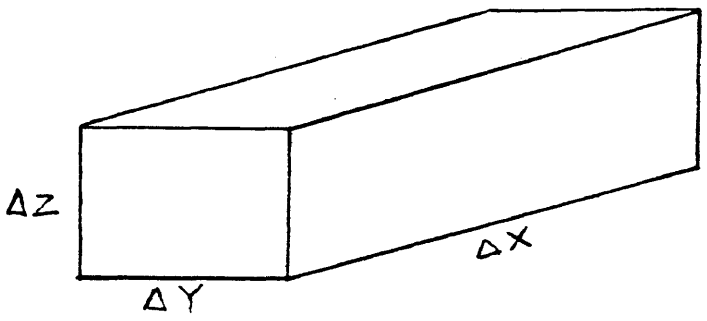

We can assume that any fluid is flowing, but oil will be considered first. Conservation of mass requires that

Mass in - mass out + generation = accumulation. (1)

We will temporarily restrict ourselves to flow in one direction to simplify the derivation. For flow in the +x direction, the amount of mass entering the elemental volume during the time Δt will be:

$$\text{Mass in} = \rho_{oR} V_{ox} \quad A\Big|_x \Delta t \tag{2}$$

where:

ρ_{oR} = oil density (in the reservoir), M/L^3

V_{ox} = velocity of oil in x direction, L/T

A = flow area, L^2

Δt = time, T

the units may be expressed in any consistent system.

Similarly,

$$\text{Mass out} = \rho_{oR} V_{ox} A\Big|_{x+\Delta x} \Delta t \tag{3}$$

The mass of the oil in the volume at any time may be expressed as:

$$\text{mass of oil} = \rho_{oR} V_B \phi S_o \tag{4}$$

where:

V_B = bulk volume ($\Delta x\ \Delta y\ \Delta z$), L^3

ϕ = porosity, L^3/L^3

S_o = oil saturation, fraction of porosity, L^3/L^3

Accumulation is equal to the mass of oil contained in the elemental volume at time t + Δt minus the mass contained in the volume at time t.

$$\text{Accumulation} = \rho_{oR}\ V_B\ \phi\ S_o\big|_{t+\Delta t} - \rho_{oR}\ V_B\ \phi\ S_o\big|_t \qquad (5)$$

The generation term represents the production of fluids from or injection of fluids into the volume. With production defined as positive, this term will be represented by

$$\text{generation} = -q_{oR}\ \rho_{oR}\ \Delta t \qquad (6)$$

where:

q_{oR} = rate of oil production at reservoir conditions, L^3/T

Substituting into Equation 1 leads to:

$$\rho_{oR}\, V_{ox} A\big|_x \;\Delta t - \rho_{oR}\, V_{ox} A\big|_{x+\Delta x} \;\Delta t - q_{oR}\, \rho_{oR}\, \Delta t =$$

$$\rho_{oR}\, V_B\, \phi\, S_o\big|_{t+\Delta t} - \rho_{oR}\, V_B\, \phi\, S_o\big|_t \qquad (7)$$

since VA = q, Equation 7 can be written as

$$\rho_{or}\, q_{ox}\big|_x - \rho_{or}\, q_{ox}\big|_{x+\Delta x} - q_{or}\, \rho_{or}\, \Delta t =$$

$$\rho_{or}\, V_B \phi\, S_o\big|_{t+\Delta t} - \rho_{or}\, V_B\, \phi\, S_o\big|_t \qquad (8)$$

The flow area is $\Delta y \Delta z$ by inspection and the bulk volume is $\Delta x \Delta y \Delta z$. If these substitutions are made and the resulting equation is divided by $\Delta x \Delta y \Delta z \Delta t$ the equation becomes:

$$\frac{\rho_{oR}\, q_{ox}\big|_x - \rho_{oR}\, q_{ox}\big|_{x+\Delta x}}{\Delta x\ \Delta y\ \Delta z} - \frac{q_{oR}\, \rho_{oR}}{\Delta x\ \Delta y\ \Delta z} = \frac{S_o\, \rho_{oR}\, \phi\big|_{t+\Delta t} - S_o\, \rho_{oR}\, \phi\big|_t}{\Delta t} \qquad (9)$$

From the definition of a derivative, the equation becomes:

$$-\frac{\partial(\rho_{oR} q_{ox})}{\partial x}\ \frac{\Delta x}{V_B} - \frac{q_{oR}\, \rho_{oR}}{V_B} = \frac{\partial(S_o\, \rho_{oR}\, \phi)}{\partial t} \qquad (10)$$

Multiplying by $-V_B$ results in

$$\frac{\partial(\rho_{oR}\, q_{ox})}{\partial x}\,\Delta x + q_{oR}\,\rho_{oR} = -\,V_B\,\frac{\partial(S_o\,\rho_{oR}\phi)}{\partial t}\,. \qquad (11)$$

Equation 11 contains three dependent variables: density, velocity, and porosity. In order to reduce the number of dependent variables, all three of these are usually related to fluid pressure. If we introduce pressure in the right hand side of Equation 11 through the chain rule, the result will be:

$$\frac{\partial(\rho_{oR}\, q_{ox})}{\partial x}\,\Delta x + q_{oR}\,\rho_{oR} = -\,V_B\,\frac{\partial(S_o\,\rho_{oR}\phi)}{\partial P}\,\frac{\partial P}{\partial t}. \qquad (12)$$

The equation of state relates the density of the oil on the surface to the density of oil in the reservoir. It is expressed as:

$$\frac{\rho_o}{\rho_{oR}} = B_o \qquad (13)$$

When Equation 13 is substituted into Equation 12 the result is

$$\frac{\partial\left(\frac{\rho_o\, q_{ox}}{B_o}\right)}{\partial x}\,\Delta x + \frac{q_{oR}\,\rho_o}{B_o} = -\,V_B\,\frac{\partial\left(\frac{S_o\,\rho_o\,\phi}{B_o}\right)}{\partial P}\,\frac{\partial P}{\partial t}\,. \qquad (14)$$

Applying the product rule to Equation 14,

$$\rho_o\,\frac{\partial\left(\frac{q_{ox}}{B_o}\right)}{\partial x}\,\Delta x + \frac{q_{ox}}{B_o}\,\frac{\partial \rho_o}{\partial x}\,\Delta x + \frac{q_{oR}\,\rho_o}{B_o} =$$

$$-\,V_B\,\rho_o\,\frac{\partial\left(\frac{S_o\,\phi}{B_o}\right)}{\partial P}\,\frac{\partial P}{\partial t} - V_B\,\frac{S_o\,\phi}{B_o}\,\frac{\partial \rho_o}{\partial P}\,\frac{\partial P}{\partial t}\,. \qquad (15)$$

In building what is known as a "Black Oil Simulator," it is further assumed that the density of the oil on the surface does not change. Therefore, $\frac{\partial \rho_o}{\partial P} = 0$. With that substitution and converting the flowrate to surface conditions using the expression $q_{op} = q_{oR} \,/\, B_o$, the resulting equation is

$$\rho_o\,\frac{\partial\left(\frac{q_{ox}}{B_o}\right)}{\partial x}\,\Delta x + \rho_o\, q_{op} = -\rho_o V_B\,\frac{\partial\left(\frac{S_o\,\phi}{B_o}\right)}{\partial P}\,\frac{\partial P}{\partial t}\,. \qquad (16)$$

Canceling ρ_o results in

$$\frac{\partial\left(\frac{q_{ox}}{B_o}\right)}{\partial x}\Delta x + q_{op} = - V_B \frac{\partial\left(\frac{S_o\,\phi}{B_o}\right)}{\partial P}\frac{\partial P}{\partial t}\,. \qquad (17)$$

Applying the product rule yields

$$\frac{\partial\left(\frac{q_{ox}}{B_o}\right)}{\partial_x}\Delta x + q_{op} = - V_B \frac{S_o\,\partial\left(\frac{\phi}{B_o}\right)}{\partial P}\frac{\partial P}{\partial t} - V_B \frac{\phi}{B_o}\frac{\partial S_o}{\partial P}\frac{\partial P}{\partial t}. \qquad (18)$$

Apply the product rule to the first term gives

$$\frac{\partial\left(\frac{q_{ox}}{B_o}\right)}{\partial x}\Delta x + q_{op} = - V_B \frac{S_o}{B_o}\frac{\partial\phi}{\partial P}\frac{\partial P}{\partial t} - V_B\,\phi S_o \frac{\partial(1/B_o)}{\partial P}\frac{\partial P}{\partial t}$$

$$- V_B \frac{\phi}{B_o}\frac{\partial S_o}{\partial P}\frac{\partial P}{\partial t}\,. \qquad (19)$$

Porosity compressibility is defined by the expression:

$$c_\phi = \frac{1}{\phi}\frac{\partial\phi}{\partial P} \qquad (20)$$

where

c_ϕ = Porosity compressibility, L^2/F.

If bulk volume doesn't change then formation compressibility is defined by

$$c_f = \frac{1}{V_p} \frac{\partial V_p}{\partial P} \tag{21}$$

and c_ϕ are equal.

Where

V_p = Pore Volume, L^3.

Making this substitution yields

$$\frac{\partial\left(\frac{q_{ox}}{B_o}\right)}{\partial x} \Delta x + q_{op} = - V_B \frac{\phi_{orig}\, C_f\, S_o}{B_o} \frac{\partial P}{\partial t} - V_B\, \phi S_o \frac{\partial (1/B_o)}{\partial P} \frac{\partial P}{\partial t}$$

$$- V_B \frac{\phi}{B_o} \frac{\partial S_o}{\partial P} \frac{\partial P}{\partial t} \tag{22}$$

Collecting terms

$$\frac{\partial\left(\frac{q_{ox}}{B_o}\right)}{\partial x} \Delta x + q_{op} = - V_B \left\{\frac{\phi_{orig}\, C_f\, S_o}{B_o} + \phi\, S_o \frac{\partial (1/B_o)}{\partial P}\right\} \frac{\partial P}{\partial t}$$

$$- V_B \frac{\phi}{B_o} \frac{\partial S_o}{\partial P} \frac{\partial P}{\partial t} \tag{23}$$

Since

$\frac{\partial S_o}{\partial P} \frac{\partial P}{\partial t} = \frac{\partial S_o}{\partial t}$ from the chain rule the equation can be written as

$$\frac{\partial\left(\frac{q_{ox}}{B_o}\right)}{\partial x} \Delta x + V_B \left\{\frac{\phi_{orig} S_o c_f}{B_o} + \phi S_o \frac{\partial\left(\frac{1}{B_o}\right)}{\partial P}\right\} \frac{\partial P}{\partial t} + q_{op} =$$

$$- V_B \frac{\phi}{B_o} \frac{\partial S_o}{\partial t} \qquad (24)$$

It is now time to introduce Darcy's Law. A common expression for the law (assuming horizontal flow) is:

$$q_{ox} = - \frac{k\, k_{ro}\, A}{\mu_o} \frac{\partial P}{\partial x} \qquad (25)$$

where:

q = flowrate, Res L^3/T

k = permeability, L^2

k_{ro} = relative permeability to oil, L^2/L^2

A = area, L^2

μ = viscosity of oil, F/L^2

$\partial P/\partial x$ = pressure gradient, $F/L^2/L$

Substituting in Equation 24

$$\frac{\partial\left(-\frac{A\ k\ k_{ro}}{\mu_o\ B_o}\frac{\partial P}{\partial x}\right)}{\partial x}\Delta x + V_B\left\{\frac{\phi_{orig}\ S_o\ c_f}{B_o} + \phi\ S_o\ \frac{\partial\left(\frac{1}{B_o}\right)}{\partial P}\right\}\frac{\partial P}{\partial t} + q_{op}$$

$$= -V_B\ \frac{\phi}{B_o}\ \frac{\partial S_o}{\partial t} \qquad (26)$$

The first term will not be expanded because it will be simpler to formulate the finite difference equations when the time comes to do that. Equation 26 therefore is the fundamental equation defining oil flow in the reservoir. In an analogous manner, assuming that capillary pressure is negligible, the equation for water can be derived to be

$$\frac{\partial\left(-\frac{A\ k\ k_{rw}}{\mu_w\ B_w}\frac{\partial P}{\partial x}\right)}{\partial x}\Delta x + V_B\left\{\frac{\phi_{orig}\ S_w\ c_f}{B_w} + \phi\ S_w\ \frac{\partial\left(\frac{1}{B_w}\right)}{\partial P}\right\}\frac{\partial P}{\partial t} + q_{wp}$$

$$= -V_B\ \frac{\phi}{B_w}\ \frac{\partial S_w}{\partial t} \qquad (27)$$

The fundamental flow equation for gas can be derived in the same manner with the addition that gas dissolved in the oil and water must be taken into account along with the flow of free gas. Because of these complications, the equation for gas will be derived in detail.

mass in =

$$\rho_{gR}\, V_{gR} A\big|_x\, \Delta t + V_{os}\, R_s\, B_g\, \rho_{gR} A\big|_x\, \Delta t + V_{ws}\, R_{sw}\, B_g\, \rho_{gR} A\big|_x\, \Delta t \tag{28}$$

mass out is similarly defined at $x + \Delta x$.

Accumulation =

$$\rho_{gR}\, V_B\, \phi\, S_g\big|_{t+\Delta t} - \rho_{gR}\, V_B\, \phi\, S_g\big|_t$$

$$+ \frac{\rho_{gR}\, V_B\, \phi\, S_o\, R_s\, B_g}{B_o}\Big|_{t+\Delta t} - \frac{\rho_{gR}\, V_B\, \phi\, S_o\, R_s\, B_g}{B_o}\Big|_t$$

$$+ \frac{\rho_{gR}\, V_B\, \phi\, S_w\, R_{sw}\, B_g}{B_w}\Big|_{t+\Delta t} - \frac{\rho_{gR}\, V_B\, \phi\, S_w\, R_{sw}\, B_g}{B_w}\Big|_t \tag{29}$$

Generation =

$$- q_{gR}\, \rho_{gR}\, \Delta t - q_{oR}\, R_s\, B_g\, \rho_{gR}\, \Delta t - q_{wp}\, R_{sw}\, B_g\, \rho_{gR}\, \Delta t \tag{30}$$

Substituting into Equation 1, dividing by $\Delta x \Delta y \Delta z \Delta t$, substituting q for VA, and taking the limit as Δx and Δt approach zero results in

$$\frac{\partial(\rho_{gR}\, q_{gx})}{\partial x}\,\Delta x + \frac{\partial(\rho_{gR}\, q_{ox}\, R_s\, B_g)}{\partial x}\,\Delta x + \frac{\partial(\rho_{gR}\, q_{wx}\, R_{sw}\, B_g)}{\partial x}\,\Delta x$$

$$+ q_{gR}\,\rho_{gp} + q_{oR}\, R_s\, B_g\,\rho_{gR} + q_{wp}\, R_{sw}\, B_g\,\rho_{gR}$$

$$= -\frac{\partial}{\partial t}\left\{V_B\,\phi\left(\rho_{gR}\, S_g + \frac{\rho_{gR}\, S_o\, R_s\, B_g}{B_o} + \frac{\rho_{gR}\, S_w\, R_{sw}\, B_g}{B_w}\right)\right\} \qquad (31)$$

Applying the product rule to Equation 31 and substituting $\rho_{gR} = \rho_g / B_g$ yields

$$\rho_g \frac{\partial\left(\frac{q_{gR}}{B_g}\right)}{\partial x}\,\Delta x + \frac{q_{gR}}{B_g}\frac{\partial \rho_g}{\partial x}\,\Delta x$$

$$+ \rho_g \frac{\partial(q_{os}\, R_s)}{\partial x}\,\Delta x + q_{os}\, R_s \frac{\partial \rho_g}{\partial x}\,\Delta x$$

$$+ \rho_g \frac{\partial(q_{wx}\, R_{sw})}{\partial x}\,\Delta x + q_{ws}\, R_{sw} \frac{\partial \rho_g}{\partial x}\,\Delta x$$

$$\frac{q_{gR}\ \rho_g}{B_g} + q_{op}\ R_s\ \rho_g + q_{wp}\ R_{sw}\ \rho_g$$

$$= -\frac{\partial}{\partial t}\left(V_B\ \phi\ \frac{\rho_g}{B_g}\ S_g + V_B\phi\ \frac{\rho_g}{B_g}\ \frac{S_o\ R_s\ B_g}{B_o} + V_B\phi\ \frac{\rho_g}{B_g}\ \frac{S_w\ R_{sw}\ B_g}{B_w}\right) \tag{32}$$

Expanding the RHS

$$\text{RHS} = -\frac{\partial}{\partial t}\left(V_B\phi\ \rho_g\ S_g\ \frac{1}{B_g}\right) - \frac{\partial}{\partial t}\left(V_B\phi\ \rho_g\ S_o\ \frac{R_s}{B_o}\right)$$

$$-\frac{\partial}{\partial t}\left(V_B\phi\ \rho_g\ S_w\ \frac{R_{sw}}{B_w}\right) \tag{33}$$

Continuing with the product rule (assuming V_B is constant)

RHS =

$$-V_B\phi\ \frac{\rho_g}{B_g}\ \frac{\partial S_g}{\partial t} \quad - V_B\phi\ \rho_g\ S_g\ \frac{\partial\left(\frac{1}{B_g}\right)}{\partial t} \quad - V_B\phi\ \frac{S_g}{B_g}\ \frac{\partial \rho_g}{\partial t} - V_B\ \frac{\rho_g}{B_g}\ S_g\ \frac{\partial \phi}{\partial t}$$

$$-V_B\phi\ \rho_g\ \frac{R_s}{B_o}\ \frac{\partial S_o}{\partial t} \quad - V_B\ \phi\ \rho_g\ S_o\ \frac{\partial\left(\frac{R_s}{B_o}\right)}{\partial t} - V_B\ \phi\ S_o\ \frac{R_s}{B_o}\ \frac{\partial \rho_g}{\partial t}$$

$$-V_B\ \rho_g\ S_o\ \frac{R_s}{B_o}\ \frac{\partial \phi}{\partial t}$$

$$- V_B\phi\ \rho_g \frac{R_{sw}}{B_w} \frac{\partial S_w}{\partial t} - V_B\phi\ \rho_g\ S_w \frac{\partial\left(\frac{R_{sw}}{B_w}\right)}{\partial t} - V_B\phi\ S_w \frac{R_{sw}}{B_w} \frac{\partial \rho_g}{\partial t}$$

$$- V_B\ \rho_g\ S_w \frac{R_{sw}}{B_w} \frac{\partial \phi}{\partial t} \qquad (34)$$

By again assuming constant stock tank density, all of the $\frac{\partial \rho_g}{\partial t}$ disappear. Then all the ρ_g terms can be canceled in the equation. The production rate is expressed at surface conditions ($q_{gp} = q_{gR}/B_g$). Introducing pressure in the appropriate places with the chain rule and substituting for $\frac{\partial \phi}{\partial P}$ using Equation 20 results in

$$\frac{\partial\left(\frac{q_{gx}}{B_g}\right)}{\partial x} \Delta x + \frac{\partial(q_{ox}\ R_s)}{\partial x} \Delta x + \frac{\partial(q_{wx}\ R_{sw})}{\partial x} \Delta x$$

$$+ q_{gp} + q_{op}\ R_s + q_{wp}\ R_{sw}$$

$$= - V_B \frac{\phi}{B_g} \frac{\partial S_g}{\partial t} - V_B\ \phi\ S_g \frac{\partial\left(\frac{1}{B_g}\right)}{\partial P} \frac{\partial P}{\partial t} - V_B \frac{\phi_{orig}\ S_g\ c_f}{B_g} \frac{\partial P}{\partial t}$$

$$-V_B\phi \frac{R_s}{B_o} \frac{\partial S_o}{\partial t} - V_B\ \phi\ S_o \frac{\partial\left(\frac{R_s}{B_o}\right)}{\partial P} \frac{\partial P}{\partial t} - V_B \frac{\phi_{orig}\ S_o\ R_s\ c_f}{B_o} \frac{\partial P}{\partial t}$$

$$- V_B \phi \frac{R_{sw}}{B_w} \frac{\partial S_w}{\partial t} - V_B \phi S_w \frac{\partial \left(\frac{R_{sw}}{B_w}\right)}{\partial P} \frac{\partial P}{\partial t} - V_B \frac{\phi_{orig} S_w R_{sw} c_f}{B_w} \frac{\partial P}{\partial t}$$

(35)

Darcy's law is now substituted for q_{gx}, q_{ox}, and q_{wx}.

Collecting all of the terms containing $\frac{\partial P}{\partial t}$ on the LHS, the result is

$$\frac{\partial\left(-\frac{A k k_{rg}}{\mu_g B_g} \frac{\partial P}{\partial x}\right)}{\partial x} \Delta x$$

$$+ \frac{\partial\left(-\frac{A k k_{ro} R_s}{\mu_o B_o} \frac{\partial P}{\partial x}\right)}{\partial x} \Delta x$$

$$+ \frac{\partial\left(-\frac{A k k_{rw} R_{sw}}{\mu_w B_w} \frac{\partial P}{\partial x}\right)}{\partial x} \Delta x$$

$$+ q_{gp} + q_{op} R_s + q_{wp} R_{sw}$$

$$+ V_B \left\{ \phi S_g \frac{\partial \left(\frac{1}{B_g}\right)}{\partial P} + \phi S_o \frac{\partial \left(\frac{R_s}{B_o}\right)}{\partial P} + \phi S_w \frac{\partial \left(\frac{R_{sw}}{B_w}\right)}{\partial P} \right.$$

$$+ \frac{\phi_{orig}\, S_g\, c_f}{B_g} + \frac{\phi_{orig}\, S_o\, R_s\, c_f}{B_o} + \frac{\phi_{orig}\, S_w\, R_{sw}\, c_f}{B_w} \Big\} \frac{\partial P}{\partial t}$$

$$= - V_B\, \phi \left(\frac{1}{B_g} \frac{\partial S_g}{\partial t} + \frac{R_s}{B_o} \frac{\partial S_o}{\partial t} + \frac{R_{sw}}{B_w} \frac{\partial S_w}{\partial t}\right) \qquad (36)$$

Equations 26, 27, and 36 describe the flow of oil, water, and gas in the formation. It is now necessary to link these equations together. This is done by recognizing that

$$S_o + S_g + S_w \triangleq 1 \qquad (37)$$

or (taking time derivatives)

$$\frac{\partial S_o}{\partial t} + \frac{\partial S_g}{\partial t} + \frac{\partial S_w}{\partial t} = 0 \qquad (38)$$

Solving Equation 38 for $\frac{\partial S_g}{\partial t}$ and substituting in the RHS of Equation 36 yields

$$RHS = - V_B\, \phi \left(- \frac{1}{B_g} \frac{\partial S_o}{\partial t} - \frac{1}{B_g} \frac{\partial S_w}{\partial t} + \frac{R_s}{B_o} \frac{\partial S_o}{\partial t} + \frac{R_{sw}}{B_w} \frac{\partial S_w}{\partial t}\right) \qquad (39)$$

collecting terms

$$RHS = - V_B \phi \left\{ \left(\frac{R_s}{B_o} - \frac{1}{B_g} \right) \frac{\partial S_o}{\partial t} + \left(\frac{R_{sw}}{B_w} - \frac{1}{B_g} \right) \frac{\partial S_w}{\partial t} \right\} \quad (40)$$

Equation 26 is multiplied by B_o and substituted for $\phi \frac{\partial S_o}{\partial t}$, and Equation 27 is multiplied by B_w and substituted for $\phi \frac{\partial S_w}{\partial t}$.

This results in

$$\frac{\partial \left(- \frac{A\ k\ k_{rg}}{\mu_g\ B_g} \frac{\partial P}{\partial x} \right)}{\partial x} \Delta x$$

$$+ \frac{\partial \left(- \frac{A\ k\ k_{ro} R_s}{B_o\ \mu_o} \frac{\partial P}{\partial x} \right)}{\partial x} \Delta x$$

$$+ \frac{\partial \left(\frac{A\ k\ k_{rw}\ R_{sw}}{\mu_w\ B_w} \frac{\partial P}{\partial x} \right)}{\partial x} \Delta x$$

$$+ V_B \left\{ \phi\ S_g \frac{\partial \left(\frac{1}{B_g} \right)}{\partial P} + \phi\ S_o \frac{\partial \left(\frac{R_s}{B_o} \right)}{\partial P} + \phi\ S_w \frac{\partial \left(\frac{R_{sw}}{B_w} \right)}{\partial P} \right.$$

$$\left. + \phi_{orig}\ S_g \frac{c_f}{B_g} + \phi_{orig}\ S_o \frac{R_s\ c_f}{B_o} + \phi_{orig}\ S_w \frac{R_{sw}\ c_f}{B_w} \right\} \frac{\partial P}{\partial t}$$

$$+ \quad q_{gp} + \quad q_{op} R_s \quad + \quad q_{wp} R_{sw}$$

$$= \quad \left(\frac{R_s}{B_o} - \frac{1}{B_g}\right) \left\{B_o \frac{\partial\left(- \frac{A\ k\ k_{ro}}{\mu_o\ B_o} \frac{\partial P}{\partial x}\right)}{\partial x} \quad \Delta x \right.$$

$$+ \quad \left(V_B\ \phi_{orig}\ S_o\ c_f \quad + V_B\ \phi\ S_o\ B_o \frac{\partial\left(\frac{1}{B_o}\right)}{\partial P}\right) \frac{\partial P}{\partial t}$$

$$\left. + \quad q_{op}\ B_o \right\}$$

$$+ \quad \left(\frac{R_{sw}}{B_w} - \frac{1}{B_g}\right) \left\{B_w \frac{\partial\left(- \frac{A\ k\ k_{rw}}{\mu_w\ B_w} \frac{\partial P}{\partial x}\right)}{\partial x} \quad \Delta x \right.$$

$$+ \quad \left(V_B\ \phi_{orig}\ S_w\ c_f + V_B\ \phi\ S_w\ B_w \frac{\partial\left(\frac{1}{B_w}\right)}{\partial P}\right) \frac{\partial P}{\partial t}$$

$$\left. + \quad q_{wp}\ B_w \right\} \qquad (41)$$

This eliminates all terms which explicitly have saturation as the dependent variable! We are left with an equation in

which pressure is the only unknown (assuming that all the coefficients such as B_o, B_g, etc. can be specified.) The equation is re-witten so that the $\frac{\partial P}{\partial t}$ terms are the only terms on the RHS. When this is done and the terms are regrouped, the result is

$$\left\{\left(R_s - \frac{B_o}{B_g}\right) \frac{\partial\left(\frac{A\ k\ k_{ro}}{\mu_o\ B_o} \frac{\partial P}{\partial x}\right)}{\partial x} \Delta x - \frac{\partial\left(\frac{A\ k\ k_{ro}\ R_s}{\mu_o\ B_o} \frac{\partial P}{\partial x}\right)}{\partial x} \Delta x\right.$$

$$+ \left(R_{sw} - \frac{B_w}{B_g}\right) \frac{\partial\left(\frac{A\ k\ k_{rw}}{\mu_w\ B_w} \frac{\partial P}{\partial x}\right)}{\partial x} \Delta x - \frac{\partial\left(\frac{A\ k\ k_{rw}\ R_{sw}}{\mu_w\ B_w} \frac{\partial P}{\partial x}\right)}{\partial x} \Delta x$$

$$\left. - \frac{\partial\left(\frac{A\ k\ k_{rg}}{\mu_g\ B_g} \frac{\partial P}{\partial x}\right)}{\partial x} \Delta x\right\}$$

$$+ q_{gp} + q_{op} R_s + q_{wp} R_{sw}$$

$$- q_{op} R_s + q_{op} \frac{B_o}{B_g} - q_{wp} R_{sw} + q_{wp} \frac{B_w}{B_g}$$

$$= -\left\{V_B \phi\ S_o \frac{\partial\left(\frac{R_s}{B_o}\right)}{\partial P} - \left(\frac{R_s}{B_o} - \frac{1}{B_g}\right) V_B\ \phi\ S_o\ B_o \frac{\partial\left(\frac{1}{B_o}\right)}{\partial P}\right.$$

$$+ V_B \phi S_w \frac{\partial(\frac{R_{sw}}{B_w})}{\partial P} - (\frac{R_{sw}}{B_w} - \frac{1}{B_g}) V_B \phi S_w B_w \frac{\partial(\frac{1}{B_w})}{\partial P}$$

$$+ V_B \phi S_g \frac{\partial(\frac{1}{B_g})}{\partial P}$$

$$+ \frac{V_B \phi_{orig} S_o R_s c_f}{B_o} - (\frac{R_s}{B_o} - \frac{1}{B_g}) V_B \phi_{orig} S_o c_f$$

$$+ \frac{V_B \phi_{orig} S_w R_{sw} c_f}{B_w} - (\frac{R_{sw}}{B_w} - \frac{1}{B_g}) V_B \phi_{orig} S_w c_f$$

$$+ \frac{V_B \phi_{orig} S_g c_f}{B_g} \} \frac{\partial P}{\partial t} \qquad (42)$$

The terms containing c_f can be reorganized to be

$$\frac{V_B \phi_{orig} S_o R_s C_f}{B_o} - \frac{V_B \phi_{orig} S_o R_s c_f}{B_o} + \frac{V_B \phi_{orig} S_o c_f}{B_g}$$

$$+ \frac{V_B \phi_{orig} S_w R_{sw} c_f}{B_w} - \frac{V_B \phi_{orig} S_w R_{sw} c_f}{B_w} + \frac{V_B \phi_{orig} S_w c_f}{B_g}$$

$$+ \frac{V_B \phi_{orig} S_g c_f}{B_g}$$

Canceling terms leads to

$$\frac{V_B \phi_{orig} S_o c_f}{B_g} + \frac{V_B \phi_{orig} S_w c_f}{B_g} + \frac{V_B \phi_{orig} S_g c_f}{B_g}$$

Factoring out $\frac{V_B \phi_{orig} c_f}{B_g}$ and remembering that $S_o+S_w+S_g = 1$ leads to the following rearrangement of Equation 42:

$$\left(R_s - \frac{B_o}{B_g}\right) \frac{\partial\left(\frac{A k k_{ro}}{\mu_o B_o} \frac{\partial P}{\partial x}\right)}{\partial x} \Delta x - \frac{\partial\left(\frac{A k k_{ro} R_s}{\mu_o B_o} \frac{\partial P}{\partial x}\right)}{\partial x} \Delta x$$

$$+ \left(R_{sw} - \frac{B_w}{B_g}\right) \frac{\partial\left(\frac{A k k_{rw}}{\mu_w B_w} \frac{\partial P}{\partial x}\right)}{\partial x} \Delta x - \frac{\partial\left(\frac{A k k_{rw} R_{sw}}{\mu_w B_w} \frac{\partial P}{\partial x}\right)}{\partial x} \Delta x$$

$$- \frac{\partial\left(\frac{A k k_{rg}}{\mu_g B_g} \frac{\partial P}{\partial x}\right)}{\partial x} \Delta x$$

$$+ \frac{q_{op}\, B_o}{B_g} + \frac{q_{wp}\, B_w}{B_g} + q_{gp}$$

$$= -\{ V_B\phi\, S_o \frac{\partial(\frac{R_s}{B_o})}{\partial P} + (\frac{B_o}{B_g} - R_s)\, V_B\phi\, S_o \frac{\partial(\frac{1}{B_o})}{\partial P}$$

$$+ V_B\phi\, S_w \frac{\partial(\frac{R_{sw}}{B_w})}{\partial P} + (\frac{B_w}{B_g} - R_{sw})\, V_B\phi\, S_w \frac{\partial(\frac{1}{B_w})}{\partial P}$$

$$+ V_B\, \phi\, S_g \frac{\partial(\frac{1}{B_g})}{\partial P}$$

$$+ V_B \frac{\phi_{orig}\, c_f}{B_g}\} \frac{\partial P}{\partial t} \qquad (43)$$

Equation 43 is the pressure equation. It completely describes (within the limitation of the assumptions) the pressure behavior of a multiphase system flowing in one direction. It can be expanded to three dimensions by adding the appropriate $\frac{\partial P}{\partial y}$ and $\frac{\partial P}{\partial Z}$ terms to the LHS. The following

assumptions have been made in this derivation:

1) Surface oil density does not change with time.
2) PVT properties are functions of pressure only (isothermal flow).
3) Bulk volume does not change.
4) Darcy's law applies (no turbulent flow).
5) Horizontal flow.
6) Capillary pressure effects are negligible.

Equation 43 is nonlinear because the coefficients are functions of the dependent variable (pressure). In order to solve this equation, it is necessary to resort to numerical means. The technique used in this dissertation is finite differences. In using a finite difference technique the derivative $\frac{\partial P}{\partial X}$ is replaced by the difference $\frac{P_1 - P_0}{X_1 - X_0}$. By doing this, an equation which contains derivatives can be transformed into an equation which contains only individual values such as P_1. Both space and time must be divided into discreet intervals because Equation 43 contains both space and time derivatives. There are a number of methods for developing the finite difference equations (FDE). These range from fully explicit to simultaneous solutions. Various methods will be described below.

We will write the FDE for the following spatial system.

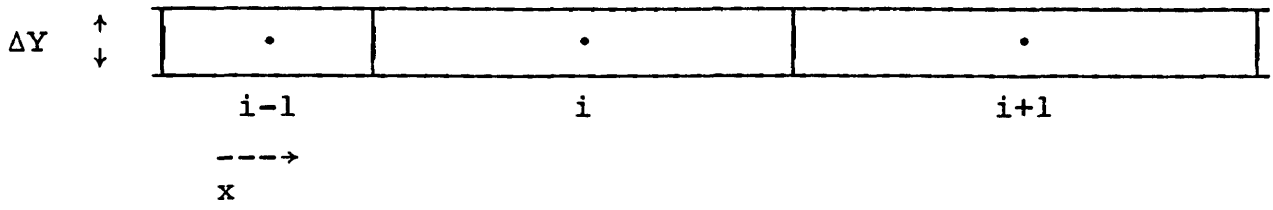

The pressures are assumed to be known in the center of each block and that pressure is the same throughout in each block. This is known as a "block centered" representation. The time domain will be described through the use of superscripts. "n" represents the current time level and "n + 1" represents the new time level at which we wish to find pressure and saturation. Thus, P_i^n represents the pressure in the cell under consideration (i) at the current time level. The three most common methods of solving the equations are explicit; implicit pressure-explicit saturation; (IMPES) and simultaneous solution.

In the explicit formulation, the new pressures are calculated for each cell individually using the old pressures in the adjoining cells. On a time space grid this could be represented as follows:

Step 1:

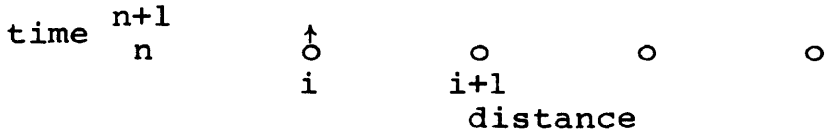

Step 2:

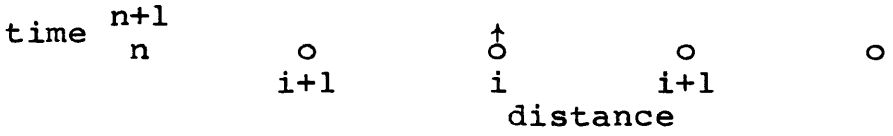

Once pressure is known at each cell for the new time level, the saturations are calculated in exactly the same manner.

In the implicit formulation we solve for all of the unknown values simultaneously. This could be represented by:

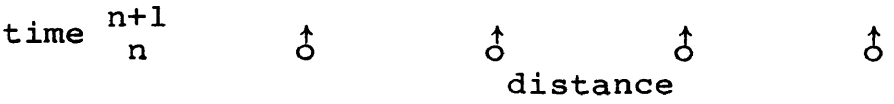

When solving implicitly, a set of equations are written for each cell resulting in a diagonally banded matrix. This matrix is then solved numerically (Gausian elimination, perhaps) to obtain the new pressure in each node simultaneously. In the IMPES method we then solve for the

saturations explicitly.

In the simultaneous solution method both pressure and saturation are calculated simultaneously. This technique results in a block diagonal matrix which is more difficult to solve. It also requires another coupling equation--usually capillary pressure.

The IMPES method was chosen in this thesis because it is more stable than the explicit method, much easier to program than the simultaneous solution method, in general use in many commercial simulators, and has been shown to give good answers in widely varying reservoirs.

The above discussion related to the manner of solving for pressure. Since the coefficients are functions of pressure (or saturation) they must be evaluated at some time level also. For a fully implicit formulation, the coefficients should be evaluated at the new pressures and saturations. This necessitates either an iterative technique or a predictor algorithm (or both). In this thesis it was decided to evaluate the coefficients at the current time level. This is known as explicit coefficients. Even though the implicit coefficient method allows larger time steps with greater stability, it does not necessarily result in greater accuracy. In fact, there is evidence in the literature that pressure dependent coefficients, at least, should

be evaluated explicitly.

Equation 43 will now be put in finite difference form using the IMPES method with explicit coefficients. To represent the pressure derivative $\frac{\partial P}{\partial x}$ we will use the form $\frac{P_i - P_{i-1}}{\frac{\Delta X_i}{2} + \frac{\Delta X_{i-1}}{2}}$. To represent $\frac{\partial P}{\partial t}$ we will use $\frac{P_i^{n+1} - P_i^n}{\Delta t}$. It is necessary to evaluate coefficients such as $\frac{A\ k\ k_{ro}}{\mu_o\ B_o}$ for flow between cells. In order to simplify the derivation, the superscript + will refer to values between cells i and i+1, and - will refer to values between cells i and i-1. With this in mind ΔX^+ can be seen to be $\frac{1}{2}\ \Delta X_i + \frac{1}{2}\ \Delta X_{i+1}$. Other items are defined as follows:

$$\Delta X^- = \frac{1}{2}\ \Delta X_i + \frac{1}{2}\ \Delta X_{i-1}$$

$$\Delta P^+ = P_{i+1} - P_i$$

$$\Delta P^- = P_{i-1} - P_i$$

$$N^+ = c\ [\frac{A\ k\ k_{ro}}{\mu_o\ B_o}]^+ / \Delta x^+$$

$$N^- = c\left[\frac{A\ k\ k_{ro}}{\mu_o\ B_o}\right]^- /\Delta X^-$$

$$G^+ = c\left[\frac{A\ k\ k_{rg}}{\mu_g\ B_g}\right]^+ /\Delta X^+$$

$$G^- = c\left[\frac{A\ k\ k_{rg}}{\mu_g\ B_g}\right]^- /\Delta X^-$$

$$W^+ = c\left[\frac{A\ k\ k_{rw}}{\mu_w\ B_w}\right]^+ /\Delta X^+$$

$$W^- = c\left[\frac{A\ k\ k_{rw}}{\mu_w\ B_w}\right]^- /\Delta X^-$$

where $c = 6.32867 \times 10^{-3}$ for units of md, ft, cp, psi.

When PVT functions have directional superscripts, the average value of the function is used. For example:

$$B_o^+ = 0.5\ (B_{oi} + B_{oi+1}) \qquad (44)$$

The only exception to this is viscosity which is considered to be a part of mobility $(\frac{k}{\mu})$. In order to evaluate mobility, the potential for each phase is calculated in each cell. The mobility for flow between two cells is selected as the value in the cell <u>from</u> which the fluid will flow. This is known as upstream weighting. By calculating mobility for each phase separately, the correct results will be

calculated when countercurrent flow occurs.

It can be seen that the coefficients will change from the beginning to the end of the time step. The pressures and saturations calculated using explicit coefficients will be in error. However, this error decreases as time step size decreases, so the easiest way to handle this problem is to decrease the time step size.

It is possible to save time in calculating the flow coefficients by breaking them into subgroups. For example:

$$N_x^+ = \left(\frac{1}{B_o}\right)^+ \left(\frac{c\, A_x\, k_x}{\Delta_x}\right)^+ \left(\frac{k_{ro}}{\mu_o}\right)^+ \qquad (45)$$

Note that $\left(\frac{c\, A_x\, k_x}{\Delta_x}\right)^+$ does not change with time. This part of the coefficient can be calculated during set-up and stored.

When Equation 43 is multiplied by V_B and written in finite difference form the result is Equation 46. Recognize that $\left(\frac{V_B}{A} = \Delta x\right)$.

$$\left(R_s - \frac{B_o}{B_g}\right)\left(\frac{N^+\Delta P^+ - N^-\Delta P^-}{\Delta x}\right)\Delta x - \left(\frac{N^+R_s{}^+\Delta P^+ - N^-R_s{}^-\Delta P^-}{\Delta x}\right)\Delta x$$

$$+ \left(R_{sw} - \frac{B_w}{B_g}\right)\left(\frac{W^+\Delta P^+ - W^-\Delta P^-}{\Delta x}\right)\Delta x - \left(\frac{W^+R_{sw}^+\Delta P^+ - W^-R_{sw}^-\Delta P^-}{\Delta x}\right)\Delta x$$

$$- \left(\frac{G^+\Delta P^+ - G^-\Delta P^-}{\Delta x}\right)\Delta x$$

$$+ q_{op}\frac{B_o}{B_g} + \frac{q_{wp}B_w}{B_g} + q_{gP}$$

$$= -\frac{A_8}{B_g}\left(\frac{P_i^{n+1} - P_i^n}{\Delta t}\right) \qquad (46)$$

where

$$A_8 = V_B\,\phi\,S_o\,B_o\,\frac{\partial\,(1/B_o)}{\partial P}$$

$$+ V_B\,\phi\,S_w\,B_w\,\frac{\partial(1/B_w)}{\partial P}$$

$$+ V_B\,\phi\,B_g\left(\frac{S_o}{B_o}\frac{\partial R_s}{\partial P} + \frac{S_w}{B_w}\frac{\partial R_{sw}}{\partial P} + S_g\frac{\partial(1/B_g)}{\partial P}\right)$$

$$+ V_B \phi_{orig} C_f \qquad (47)$$

and terms without superscripts of + or - refer to cell i.

Expanding and reorganizing Equation 47 gives:

$$\left(R_s N^+ - \frac{B_o}{B_g} N^+ - R_s^+ N^+ + R_{sw} W^+ - \frac{B_w}{B_g} W^+ - R_{sw}^+ W^+ - G^+\right)\Delta P^+$$

$$\left(-R_s N^- + \frac{B_o}{B_g} N^- + R_s^- N^- - R_{sw} W^- + \frac{B_w}{B_g} W^- + R_{sw}^+ W^- + G^-\right)\Delta P^-$$

$$+ \frac{q_{op} B_o}{B_g} + \frac{q_{wp} B_w}{B_g} + q_{gp}$$

$$= - \frac{A_8}{B_g} \left(\frac{P_i^{n+1} - P_i^n}{\Delta t}\right) \qquad (48)$$

We define 0^+ as follows:

$$\begin{aligned} 0^+ = {} & (B_g R_s^+ - R_s B_g + B_o) N^+ \\ & + (B_g R_{sw}^+ - R_{sw} B_g + B_w) W^+ \\ & + B_g G^+ \end{aligned} \qquad (49)$$

Multiplying Equation 48 by $-B_g$ and substituting Equation 49

$$0^{+}\Delta P^{+} + 0^{-}\Delta P^{-} + A_9 = A_8 \left(\frac{P_i^{n+1} - P_i^{n}}{\Delta t}\right) \tag{50}$$

where

$$A_9 = - q_{op} B_o - q_{wp} B_w - q_{gp} B_g \tag{51}$$

Any further breakdown of Equation 50 depends on the solution method to be used. In this thesis, a form of Gausian elimination which is very efficient for banded matrices was used. Line successive over relaxation (LSOR) was also tried, but for the small problems in this thesis, a direct elimination method was faster and assured that there was no convergence error. When using the matrix solution, greater precision can be obtained by solving for "residuals" instead of pressures. The application of Equation 50 in this case is as follows:

The general solution process is

$$[A]\ [P] = [B] \tag{52}$$

This equation is solved for the vector P. By converting to residual form the equations may be written as

$$p^{n+1} = p^n + \varepsilon \tag{53}$$

where ε is the difference between the old and new pressures. Substituting Equation 53 into Equation 52 gives

$$[A]\,[p^n] + [A]\,[\varepsilon] = [B] \tag{54}$$

or

$$[A]\,[\varepsilon] = [B] - [A]\,[p^n] \tag{55}$$

Equation 50 is rearranged as follows:

$$o^+p_{i+1} - o^+p_i + o^-p_{i-1} - o^-p_i + A_9 = \frac{A_8}{\Delta t}\,p_i^{n+1} - \frac{A_8}{\Delta t}\,p_i^{n} \tag{56}$$

In an implicit pressure formulation the pressures on the left hand side are defined at time level n+1. Collecting terms

$$o^-p_{i-1}^{n+1} - (o^+ + o^- + \frac{A_8}{\Delta t})\,p_i^{n+1} + o^+p_{i+1}^{n+1} = -\,(A_9 + \frac{A_8}{\Delta t}\,p_i^{n}) \tag{57}$$

By defining the terms appropriately Equation 57 can be written as

$$a_i P_{i-1}^{n+1} + b_i P_i^{n+1} + c_i P_{i+1}^{n+1} = d_i \qquad (58)$$

When Equation 58 is written for all cells, a tridiagonal matrix results (the following example is for four cells)

$$\begin{matrix} b_1 & -c_1 & 0 & 0 \\ -a_2 & b_2 & -c_2 & 0 \\ 0 & -a_3 & b_3 & -c_3 \\ 0 & 0 & -a_4 & b_4 \end{matrix} \begin{matrix} P_1 \\ P_2 \\ P_3 \\ P_4 \end{matrix} = \begin{matrix} d_1 \\ d_2 \\ d_3 \\ d_4 \end{matrix} \qquad (62)$$

When Equation 57 is written in residual form, the matrix becomes

$$\begin{matrix} b_1 & -c_1 & 0 & 0 \\ -a_2 & b_2 & -c_2 & 0 \\ 0 & -a_3 & b_3 & -c_3 \\ 0 & 0 & -a_4 & b_4 \end{matrix} \begin{matrix} \varepsilon_1 \\ \varepsilon_2 \\ \varepsilon_3 \\ \varepsilon_4 \end{matrix} = \begin{matrix} e_1 \\ e_2 \\ e_3 \\ e_4 \end{matrix}$$

where

$$e_i = d_i - (a_i + b_i + c_i)\ P_i^n$$

It requires little extra work to write the equations in residual form and a great benefit is reaped -- the residual may be solved for in single precision rather than double precision. This reduces the computer time by 30 percent to 40 percent.